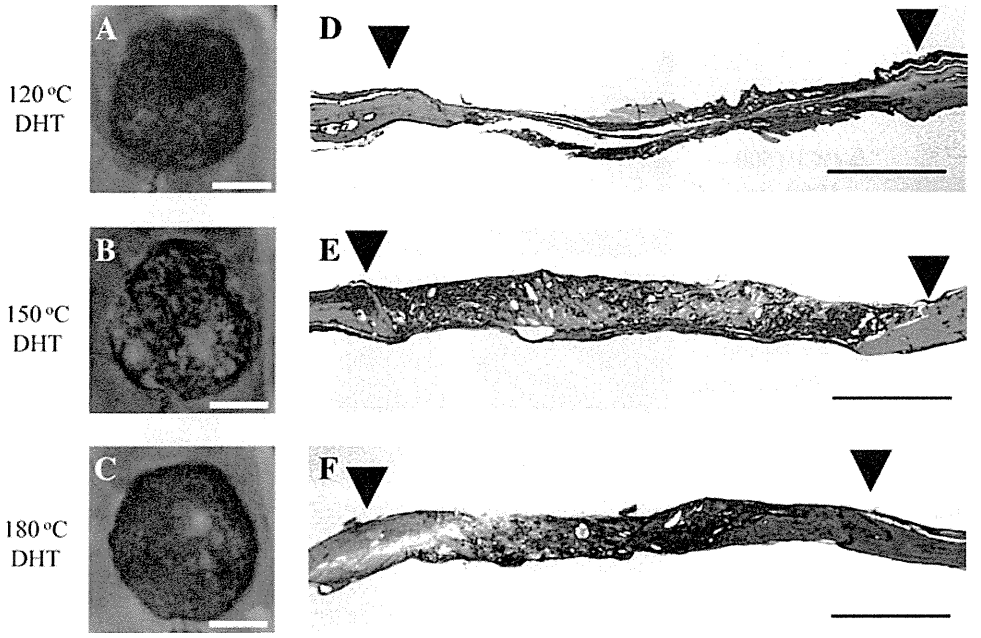

FIG. 2. Radiographic examination and histological overview of the implants in week 12. **(A, D)** OCP/Col with 120°C DHT, **(B, E)** OCP/Col with 150°C DHT, and **(C, F)** OCP/Col with 180°C DHT. ▼, defect margin. Bars = 4 mm **(A–C)**, 2 mm **(D–F)**. Color images available online at www.liebertonline.com/tea

Bone regeneration of OCP/Col with different temperature of DHT

We previously reported that DHT during the fabrication of OCP/Col influences bone regeneration by OCP/Col.[40] New bone formation by OCP/Col with DHT was significantly higher than that without DHT,[40] although it is unclear whether the temperature of the DHT is optimized with regard to the osteoconductive characteristics of OCP/Col. Bone regeneration by the implantation of OCP (300-500 μm)/Col with different DHT (120°C, 150°C, and 180°C) was compared. The results of the radiographic examination are shown in Figure 2 (A-C). At week 12, there was moderate radiopacity in the defect implanted with OCP/Col with 120°C DHT (Fig. 2A). In OCP/Col with 180°C DHT (Fig. 2C), the radiopacity was higher than that in OCP/Col with 120°C DHT, but the area of radiopacity was smaller than the defect. In OCP/Col with 150°C DHT (Fig. 2B), a larger area of thorn-like radiopacity amalgamated and condensed.

An overview of histological sections at week 12 is shown in Figure 2D-F. New bone formation of OCP/Col with 120°C DHT was limited to the defect margin and around the implanted OCP (Fig. 2D). In OCP/Col with 180°C DHT (Fig. 2F), newly formed bone was observed sporadically in the defect. The area of newly formed bone was larger than that with OCP/Col with 120°C DHT. In OCP/Col with 150°C DHT (Fig. 2E), newly formed bone was observed throughout the defect and surrounding the remaining OCP. The area of newly formed bone of OCP/Col with 150°C DHT was larger than that in other samples.

Radiographic examination of OCP/Col with different granule size of OCP

As described above, the OCP/Col with 150°C DHT enhanced bone regeneration more than that with 120°C or 180°C DHT. Therefore, OCP/Col with 150°C DHT was evaluated further. The size effect of OCP granules (53-300 μm, 300-500 μm, or 500-1,000 μm) in Col was examined. The results of the radiographic examination are shown in Figure 3. In OCP/Col, thorn-like radiopaque masses were scattered throughout the defect in week 4 and condensed in weeks 8 and 12, and newly formed bone was observed in a large area of the defect. In particular, in 53- to 300-μm OCP/Col, the amalgamated radiopacity was more condensed and became larger than that of other samples. In Col, isolated pudgy radiopacities were scattered throughout the defect. In untreated defects, radiopacity was observed along the defect margins.

Histological examination of OCP/Col with different granule size of OCP

An overview of the histological sections (Fig. 4) showed that bone regeneration in the Col-treated group and the untreated control was limited to the margin of the defect, and most of the defect was filled with fibrous connective tissue. In OCP/Col, newly formed bone in the defect became abundant in week 12. The area of newly formed bone of 53- to 300-μm OCP/Col was the largest of the samples.

Histomorphometric examination

Histomorphometric findings regarding n-Bone% are shown in Figure 5. By week 4, mean n-Bone% ± SD in the 500- to 1,000-μm OCP/Col-treated, 300- to 500-μm OCP/Col-treated, 53- to 300-μm OCP/Col-treated, Col-treated, and untreated groups was 16.3 ± 3.9, 17.9 ± 3.3, 23.0 ± 3.2, 6.4 ± 1.6, and 6.0 ± 1.6, respectively. A significant difference was observed between the 53- to 300-μm OCP/Col-treated and other groups. By week 8, the mean n-Bone% ± SD in 500- to 1000-μm OCP/Col-treated, 300- to 500-μm OCP/Col-treated, 53- to 300-μm OCP/Col-treated, Col-treated, and untreated groups was 37.3 ± 2.2, 38.0 ± 2.0, 53.2 ± 2.7, 15.3 ± 3.6, and 9.8 ± 3.3, respectively. A significant difference was observed between the 53- to 300-μm OCP/Col-treated and other groups. By week 12, the mean n-Bone% ± SD in the 500- to 1,000-μm OCP/Col-treated, 300- to 500-μm OCP/Col-treated, 53- to 300-μm OCP/Col-treated, Col-treated, and untreated groups was 56.1 ± 2.8, 53.7 ± 3.1, 65.5 ± 3.1,

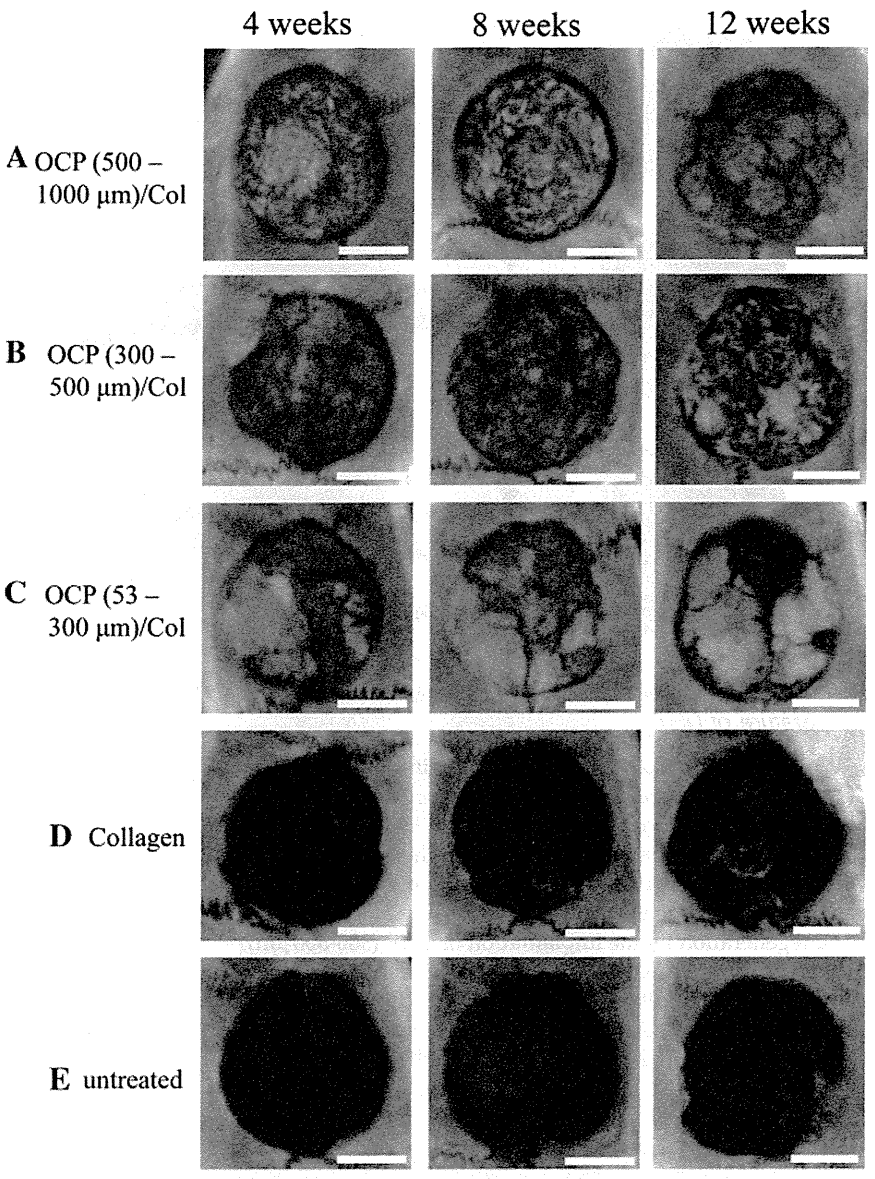

FIG. 3. Radiographs of rat calvarial defects with implantation of **(A)** 500- to 1,000-μm OCP/Col, **(B)** 300- to 500-μm OCP/Col, **(C)** 53- to 300-μm OCP/Col, and **(D)** Col; **(E)** untreated control. Dehydrothermal treatment was 150°C. Bars = 4 mm.

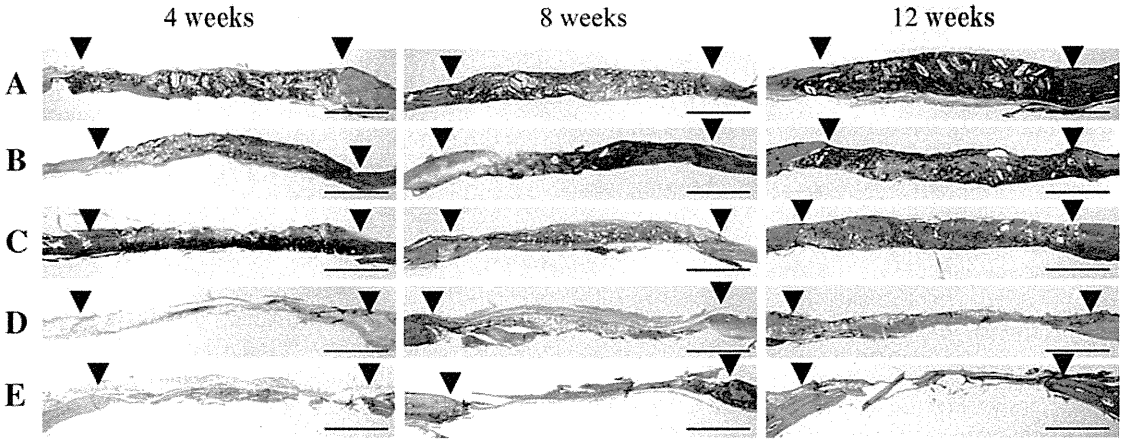

FIG. 4. Overview of the sections stained with hematoxylin and eosin: **(A)** 500- to 1,000-μm OCP/Col, **(B)** 300- to 500-μm OCP/Col, **(C)** 53- to 300 μm OCP/Col, **(D)** Col, and **(E)** untreated control. The implantation terms were 4, 8, and 12 weeks long. Dehydrothermal treatment was 150°C. ▼, defect margin. Bars = 2 mm. Color images available online at www.liebertonline.com/tea

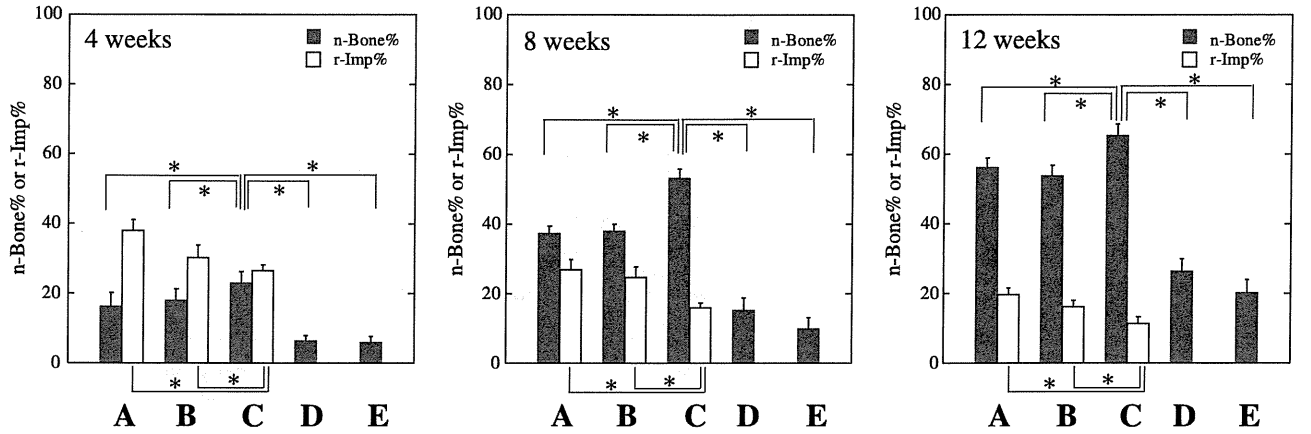

FIG. 5. Quantitative analysis of percentage of new bone in the defect (n-Bone%) and remaining implant (r-Imp%). **(A)** 500- to 1,000-μm OCP/Col, **(B)** 300- to 500-μm OCP/Col, **(C)** 53- to 300-μm OCP)/Col, **(D)** Col, and **(E)** untreated control. Data are means ± standard deviations. *$p < 0.01$.

26.4±3.6, and 20.2±3.8, respectively. A significant difference was observed between the 53- to 300-μm OCP/Col-treated and other groups.

Histomorphometric findings regarding r-Imp% are shown in Figure 5. By week 4, the mean r-Imp%±SD in the 500- to 1,000-μm OCP/Col-treated, 300- to 500-μm OCP/Col-treated, and 53- to 300-μm OCP/Col-treated groups was 38.0±3.1, 30.3±3.6, and 26.5±1.7, respectively. A significant difference was seen between OCP/Col composites. By week 8, the mean r-Imp%±SD in the 500- to 1,000-μm OCP/Col-treated, 300- to 500-μm OCP/Col-treated, and 53- to 300-μm OCP/Col-treated groups was 26.9±3.0, 24.7±3.1, and 16.0±1.4, respectively. A significant difference was seen between OCP/Col composites. By week 12, the mean r-Imp%±SD in the 500- to 1,000-μm OCP/Col-treated, 300- to 500-μm OCP/Col-treated, and 53- to 300-μm OCP/Col-treated groups was 19.6±1.9, 16.1±1.9, and 11.4±1.9, respectively. A significant difference was seen between OCP/Col composites.

TRAP staining

Representative TRAP staining at 4 weeks is shown in Figure 6. TRAP-positive multinucleated giant cells (MNGCs) were observed in close association with OCP granules, indicating that TRAP-positive osteoclast-like cells directly resorb OCP granules within the Col matrix. Sparse TRAP-positive cells were seen within the implant, in particular around 53- to 300-μm OCP granules (Fig. 6c, F).

Structural changes of OCP in vivo

Figure 7 shows the XRD patterns of the OCP/Col before (Fig. 7C, E, G) and after (Fig. 7B, D, F) implantation in rat calvarial defects. The structure of OCP tended to convert to

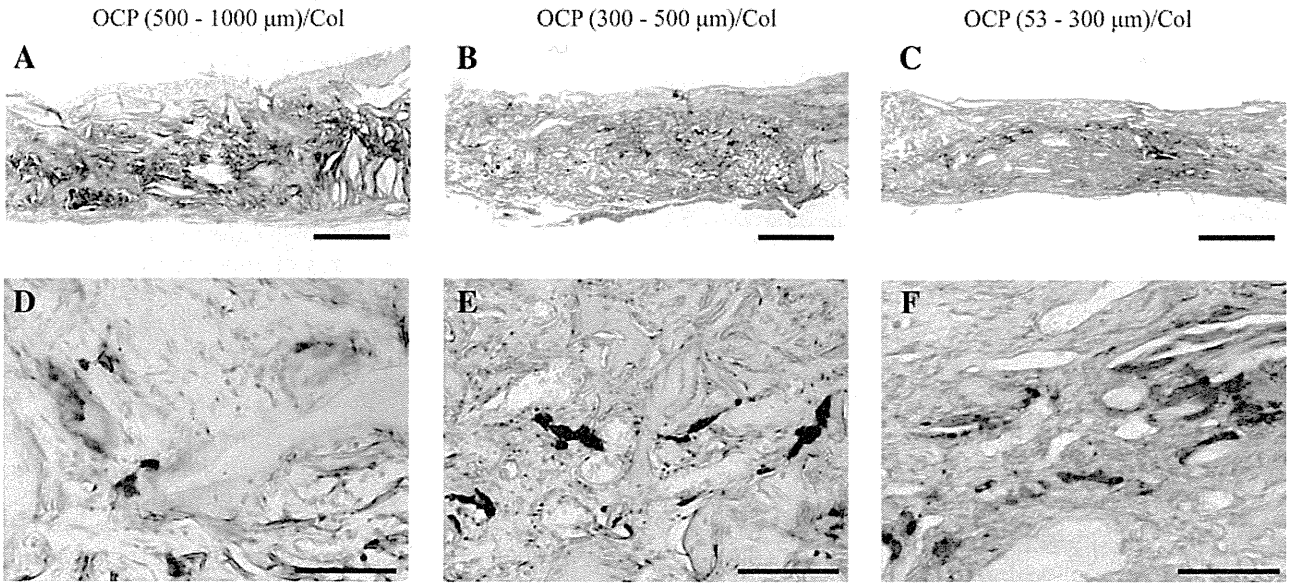

FIG. 6. Detection of tartrate-resistant acid phosphatase (TRAP)-positive multinucleated giant cells (MNGCs) around OCP granules. TRAP staining at 4 weeks: **(A, D)** 500- to 1,000-μm OCP/Col, **(B, E)** 300- to 500-μm OCP/Col, and **(C, F)** 53- to 300-μm OCP/Col. Bars = 500 μm **(A,B,C)**, 200 μm **(D,E,F)**. Color images available online at www.liebertonline.com/tea

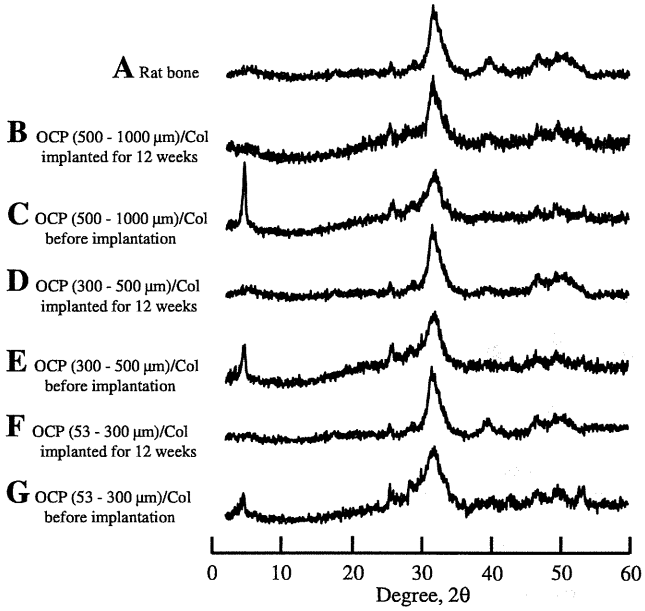

FIG. 7. X-ray diffraction patterns of **(A)** rat bone and **(B)** 500- to 1,000-μm OCP/Col implanted into rat calvarial defects at 12 weeks, **(C)** 500- to 1,000-μm OCP/Col before implantation, **(D)** 300- to 500-μm OCP/Col implanted, **(E)** 300- to 500-μm OCP)/Col before implantation, **(F)** 53- to 300-μm OCP/Col implanted, and **(G)** 53- to 300-μm OCP/Col before implantation.

that of HA with a reduction in (100) reflection intensity. The results confirmed that OCP in a Col matrix tended to convert to an apatite structure by implantation into rat bone; these changes were identical to the structural changes observed by implantation into rat calvaria,[19] mouse calvaria,[22] and subcutaneous tissue.[30]

Characterization of OCP/Col disks

Figure 8 shows scanning electron micrographs of the OCP/Col disks. The granules in the Col matrix showed an irregular morphology consisting of an aggregate form of OCP crystals (Fig. 8a-C). The pore size distributions from the mercury porosimetry data are shown in Figure 9. All disks were porous and had pore size distributions with almost the same median pore sizes (~30 μm). The scanning electron micrograph figures have structures that coincide with the mercury porosimetry pore size distribution (Fig. 8d-F).

Dissolution of OCP granules in media

Figure 10 shows the results of chemical analyses of the supernatants of the OCP/Col after 3 days of incubation with αMEM at 37°C. The Ca^{2+} concentration of the supernatant of the OCP/Col was less than that of Col and control (Fig. 10A). Conversely, the Pi concentration of the supernatant of the OCP/Col was greater than those of Col and control and was greater with smaller size of the OCP granules (Fig. 10B). Table 1 shows the DS of the media before and after the immersion of OCP/Col composites. The results showed that DS in all media examined were supersaturated with respect to HA and slightly supersaturated with respect to OCP but undersaturated with respect to DCPD. DS of Col was compatible with that of the control (medium without immersing the materials) and higher than those of OCP/Col composites with respect to HA and OCP. DS of OCP/Col (53-300 μm) was somewhat smaller than those of 300- to 500-μm and 500- to 1,000-μm OCP/Col with respect to HA and OCP, indicating that 53- to 300-μm OCP granules in Col matrix had a higher potential to dissolve and tended to form HA and possibly OCP.

Discussion

The present study provides evidence that the granule size of OCP dispersed in a Col matrix greatly affects the capability of bone regeneration of OCP/Col and the degree of resorption of this composite material. The OCP/Col with the smallest OCP granules (53-300 μm) enhanced the bone regeneration rate in a rat critical-sized calvaria defect more than those with OCP granules with larger ranges (300-500 and 500-1,000 μm). The resorption of OCP/Col was also more enhanced in the composite including the smallest OCP granules (53-300 μm) than in other OCP/Col composites with larger OCP granules. The thermal dehydration of OCP/Col under vacuum conditions, a measure to cross-link atelo-Col fibrils,[41] reconfirmed that the bone regeneration is supported most efficiently if the treatment is performed under certain conditions.[40] The present study focused on an OCP/Col composite treated at 150°C, which revealed higher bone regenerative capability. The amount of cross-linking was greater with higher dehydrothermal temperature.[41] The extent of the cross-linking in Col may affect the material characteristics[42] and regulate the capacity of bone regeneration by the present composite materials. The OCP/Col materials were well characterized to interpret the biological response in a rat critical-sized calvaria defect. The OCP structure gradually collapses if heated in air from 150°C to 200°C,[32,33] but the present DHT, which was heated to 180°C under vacuum conditions, did not induce full decomposition of the OCP structure, at least by the estimation in XRD. The X-ray pattern of OCP in the Col matrix became somewhat broader with smaller granule size, which could be due to the decrease in the crystal orientation within the Col matrix. The mercury intrusion porosimetry of the OCP/Col showed that the pore distribution was relatively homogenous (~30 μm) regardless of the granule size of OCP. The material characterization indicated that the biological responses of OCP/Col can be evaluated as a function of the granule size of OCP under which other parameters of the material are relatively constant.

A radiograph of the OCP/Col implantation showed that radiopacity progressively increases sporadically and the calcified matter fuses throughout the defect time dependently. Our previous studies indicated that bone formation is initiated from OCP granule surface,[22,30,43] although bone formation is also observed from the margin of the defect.[19,43] Bone formation is not induced if OCP is implanted in mouse abdominal subcutaneous tissue near fascia.[30] The present histological findings supported the observation that OCP granules work as a nucleation site for bone regeneration. The OCP granules in Col matrix were detected as hematoxylinophilic substances, which have been confirmed to stem from the accumulation of matrix proteins,[22] including circulating serum proteins,[30] within the space formed by each OCP crystal. Previous studies suggested that bone

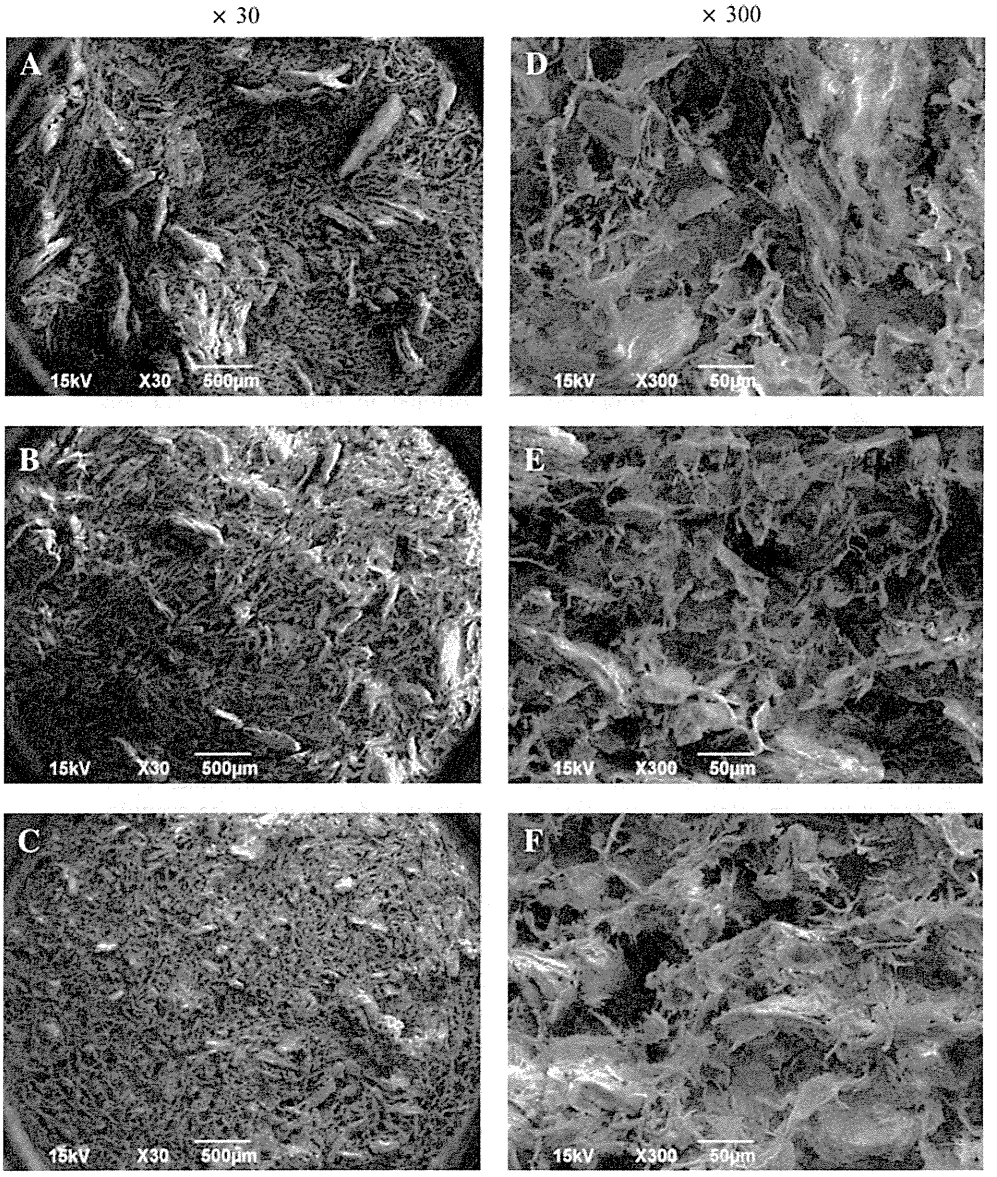

FIG. 8. Scanning electron micrographs of OCP/Col disks. **(A, D)** 500- to 1,000-μm OCP/Col, **(B, E)** 300- to 500-μm OCP/Col, and **(C, F)** 53- to 300-μm OCP/Col. Bars = 500 μm **(A,B,C)**, 50 μm **(D,E,F)**.

regeneration starts from the surface of the structure composed of OCP crystals and matrix proteins,[22] which is formed by implanting the OCP granules into bone tissue. Although Col is a cell-attaching biological molecule,[44] the present Col disks did not result in greater bone formation than OCP/Col. The results suggest that the major contribution in enhancing bone formation may stem from the capacity of OCP crystals to stimulate host osteoblastic cells to differentiate.[17,19] The fact that the capacity of bone regeneration differs depending on granule size suggests the following mechanisms; a reduction in the granule size within the unit volume of the Col matrix increases the nucleation site for new bone and some physicochemical change in relation to the granule size could enhance bone regeneration. The advancement of bone formation by 53- to 300-μm OCP/Col resulted in fusion of new bone that could be nucleated from the OCP granules within Col matrix.

XRD analysis of the retrieved tissue with OCP/Col implants indicated that OCP tends to convert to HA until 12 weeks after implantation, although XRD showed the remnant OCP unresorbed and the newly formed bone.[23] The conversion from OCP to HA induces physicochemical changes with advancement of the conversion[5,19,45] and enhances osteoblastic differentiation of mouse bone marrow stromal cells together with an increase in differentiation markers, such as alkaline phosphatase (ALP) and osterix messenger RNA, in *in vitro* analyses.[17-19,46] Therefore, the granules of OCP in OCP/Col in the present study may affect bone regeneration to some extent regardless of granule size. The dissolution test of OCP/Col in a medium indicated that calcium ions tended to decrease, whereas inorganic phosphate ions tended to increase with smaller granule size. The conversion from OCP to HA *in vitro* accompanied these changes in ion concentration.[5,17,45] On the other hand, the surface area of OCP granules in Col matrix should be greater with smaller granule size because the same weight of OCP granules is included in the unit volume of the Col. The decrease in DS with respect to HA and OCP in the medium with 53- to 300-μm OCP/Col suggests that the smallest OCP granules in Col tend to convert to HA more readily than the

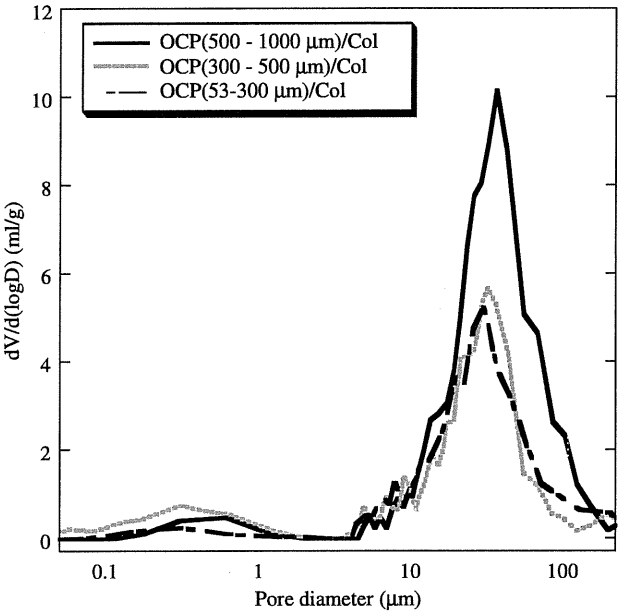

FIG. 9. Mercury porosimetry pore size distribution of 500- to 1,000-μm OCP/Col, 300 to 500-μm OCP/Col, and 53- to 300-μm OCP/Col.

larger granules. If the enhancement of the conversion from OCP to HA detected *in vitro* is reflected at the implantation site, then the stimulatory effect by the conversion from OCP to HA[19] might be involved in bone regeneration.

The resorption rate of OCP/Col was greater with smaller OCP granule size. As discussed above, one of reasons for earlier resorption could be the physicochemical factor that smaller granules of OCP are expected to have a higher specific surface area[28] in the unit volume in OCP/Col and, therefore, tend to dissolve faster than larger granules of OCP. Histochemical analysis revealed that TRAP staining was qualitatively higher in OCP/Col with smaller OCP granules than in that with larger granules. It has been proved that osteoclast formation can be induced on OCP coating from *in vitro* co-culturing in osteoblasts and bone marrow cells even in the absence of vitamin D_3, a factor to increase osteoclast-inducing factor RANKL in osteoblasts,[16] and that TRAP-positive osteoclast-like cells resorb OCP granules.[47,48] The present results reconfirmed that osteoclast-like cells can resorb OCP granules and suggest that decreasing the granule size of OCP enhances the osteoclastic cellular activity to resorb.

The effect of granule size in HA, β-TCP, and glass ceramics on bone formation has been seen in rabbit bone marrow.[49] It is becoming clear that the type of materials and granule size should be factors in the control of reactive bone formation.[9,10] HA is the most-thermodynamic stable basic salt in the physiological environment.[5] HA particles from 1 to 3 μm[49] or nano-HA deposited Col[12] have biodegradable properties if implanted in bone defects. The size of HA particles, ranging from submicron size to approximately 800 μm in diameter, affects the biological response to fibroblasts and myoblasts.[50] The size between the nano- and micrometer ranges also has an influence on osteoblast differentiation.[51] A previous histomorphometric analysis of mouse critical-sized calvaria defects revealed that OCP granules with the same granule size as those in the present study but not including the Col matrix enhanced bone formation and the appearance of TRAP-positive cells around OCP granules with larger OCP granule size; this is in contrast to the present results. In this previous study, it was easier for osteoblasts to invade, proliferate, and differentiate within the space formed by OCP granules by increasing granule size.[28] Although the effect of the granule size was opposite between the present (in the presence of Col) and previous (in the absence of Col) results,[28] the enhancement of bone regeneration was coupled with the increase in TRAP activity of osteoclast-like cells in these two observations. A similar coupling-like response to OCP granules has been found in rabbit bone marrow implantation[47] and mouse calvaria onlay graft,[52] suggesting that the enhancement of bone regeneration by OCP granules includes the activation of osteoclast-like cells around the granules during bone formation by osteoblasts. Furthermore, bone formation–related genes, such as osteocalcin, Col 1, osteopontin, and ALP, have been detected together with osteoclast-related genes, such as TRAP and Cathepsin-K in rat tibia bone marrow tissue with OCP implantation.[21]

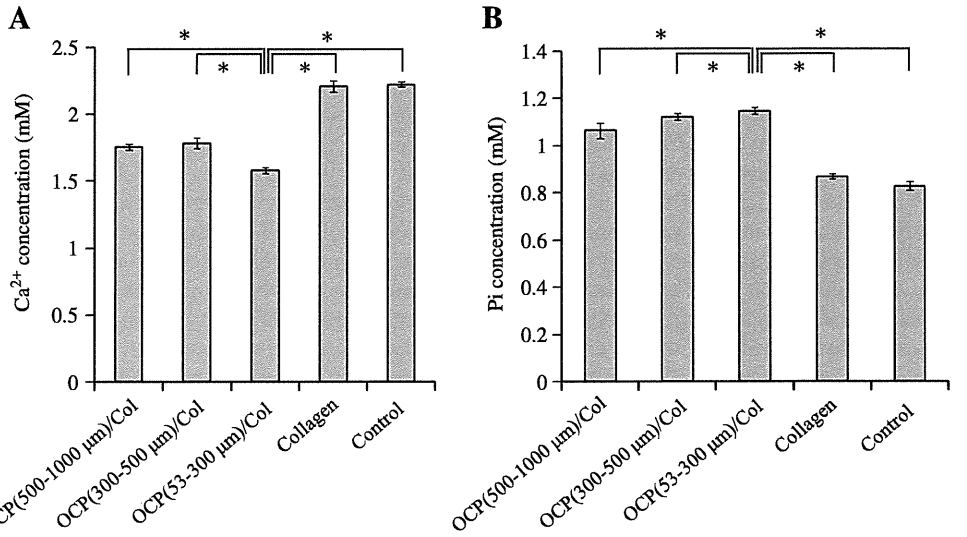

FIG. 10. Changes in the Ca^{2+} **(A)** and Pi **(B)** concentrations of alpha minimum essential medium at 37°C after 3 days of incubation of OCP/Col.

TABLE 1. SOLUTION COMPOSITION AND ITS SATURATION LEVELS AFTER INCUBATION IN αMEM.

Materials	*Calcium (mM)*	*Phosphate (mM)*	*Degree of Supersaturation*		
			HA	*OCP*	*DCPD*
OCP (500-1000 μm)/Col	1.76±0.02	1.07±0.03	3.11×10^{11}	1.04×10^{3}	5.51×10^{-1}
OCP (300-500 μm)/Col	1.78±0.04	1.12±0.01	3.85×10^{11}	1.27×10^{3}	5.87×10^{-1}
OCP (53-300 μm)/Col	1.58±0.02	1.15±0.01	2.34×10^{11}	8.69×10^{2}	5.38×10^{-1}
Collagen	2.21±0.04	2.22±0.02	5.27×10^{11}	1.39×10^{3}	5.62×10^{-1}
Control (Medium)	2.22±0.02	0.83±0.01	4.70×10^{11}	1.24×10^{3}	5.39×10^{-1}

Concentration of calcium and phosphate was expressed as average±SD by three determinations.
αMEM, α minimal essential medium; HA, hydroxyapatite; OCP, octacalcium phosphate; DCPD, dicalcium phosphate dihydrate; col, collagen.

The present study using rat critical-sized calvaria showed that OCP/Col composite can be optimized for use in the repair of defects if a smaller OCP granule size (53-300 μm) is used in the composite. From the viewpoint of the quality of regenerated bone, complete resorption of OCP granules concomitantly with replacement with new bone may be desirable.[2] OCP granules in the present study were not resorbed fully and remained even when OCP/Col with the smallest granules was used and the implantation was conducted over prolonged periods. HA is the thermodynamically most-stable salt in various calcium phosphates,[5] so the converted HA from OCP should have lower solubility than the original OCP, as revealed in a previous *in vitro* study under physiological conditions.[45] Converted HA from an OCP onlay implanted in rat calvaria is carbonate-containing HA.[53] Carbonate-containing HA is thought to be an analogue to biological apatite crystals in bone[54-56] and, therefore, exhibits higher osteoclastic cellular resorbability.[11,57,58] The osteoclastic resorption of OCP/Col composite is remarkably accelerated under mechanical conditions *in vivo*[53,59] and *in vitro*.[59] Alleviation of the mechanical stress reduces this marked osteoclastic activity, resulting in restoring the bone-regenerative property.[59] The use of a OCP/Col composite in a load-bearing site is therefore challenging. The acquisition of the ability to be fully resorbed and replaced with new bone in various implantation sites is a problem to be solved from the materials science and chemistry viewpoints and would lead to the development of an OCP-based bone substitute material that is compatible with autologous bone.

Conclusion

The present study showed that the granule size of OCP can modify the bone regenerative property of a bone substitute material consisting of OCP granules and a Col matrix. Decreasing the OCP granule size to 53 to 300 μm in a OCP/Col composite enhanced its capability to regenerate new bone relative to the larger sizes of OCP. The physicochemical property induced by the difference of the granule size may be a determinant of the bone regenerative property of OCP/Col. It appears that bone regeneration is coupled with enhanced osteoclastic resorption of OCP granules in OCP/Col. Recent studies clarified that OCP exhibits a variety of biological responses depending on the crystal chemistry.[21,48] The present study provides a clue to increase the osteoconductivity of OCP/Col by stimulating host osteoblastic cells, leading to the development of a highly osteoconductive bone substitute material and a scaffold for a tissue construct with exogenous cells approaching the performance of autologous bone.

Acknowledgments

This study was supported in part by grants in aid 17076001, 19390490, 23390450, 23659999, and 23106010 from the Ministry of Education, Science, Sports, and Culture of Japan and the Suzuken Memorial Foundation.

Disclosure Statement

No conflicting financial interests exist.

References

1. Tamai, N., Myoui, A., Tomita, T., Nakase, T., Tanaka, J., Ochi, T., and Yoshikawa, H. Novel hydroxyapatite ceramics with an interconnective porous structure exhibit superior osteoconduction in vivo. J Biomed Mater Res **59**, 110, 2002.
2. Ghanaati, S., Barbeck, M., Orth, C., Willershausen, I., Thimm, B.W., Hoffmann, C., Rasic, A., Sader, R.A., Unger, R.E., Peters, F., and Kirkpatrick, C.J. Influence of beta-tricalcium phosphate granule size and morphology on tissue reaction in vivo. Acta Biomater **6**, 4476, 2010.
3. LeGeros Rz. Properties of osteoconductive biomaterials: calcium phosphates. Clin Orthop **72**, 81, 2002.
4. Ogose, A., Hotta, T., Kawashima, H., Kondo, N., Gu, W., Kamura, T., and Endo, N. Comparison of hydroxyapatite and beta tricalcium phosphate as bone substitutes after excision of bone tumors. J Biomed Mater Res B Appl Biomater **72**, 94, 2005.
5. Brown WE, Mathew M, and Tung MS. Crystal chemistry of octacalcium phosphate. Prog Cryst Growth Charact **4**, 59, 1981.
6. Chow L. Solubility of calcium phosphates. In: Chow, L.C., and Eanes, E.D. Octacalcium Phosphate. Basel, Switzerland: Karger, 2001, pp. 94–111.
7. Bucholz RW. Nonallograft osteoconductive bone graft substitutes. Clin Orthop **395**, 44, 2002.
8. Papangkorn, K., Yan, G., Heslop, D.D., Moribe, K., Baig, A.A., Otsuka, M., and Higuchi, W.I. Influence of crystallite microstrain on surface complexes governing the metastable equilibrium solubility behavior of carbonated apatites. J Colloid Interface Sci **320**, 96, 2008.
9. Okuda, T., Ioku, K., Yonezawa, I., Minagi, H., Gonda, Y., Kawachi, G., Kamitakahara, M., Shibata, Y., Murayama, H., Kurosawa, H., and Ikeda, T. The slow resorption with replacement by bone of a hydrothermally synthesized pure calcium-deficient hydroxyapatite. Biomaterials **29**, 2719, 2008.
10. Okuda, T., Ioku, K., Yonezawa, I., Minagi, H., Kawachi, G., Gonda, Y., Murayama, H., Shibata, Y., Minami, S., Kamihira, S., Kurosawa, H., and Ikeda, T. The effect of the microstructure of beta-tricalcium phosphate on the metabolism of subsequently formed bone tissue. Biomaterials **28**, 2612, 2007.

11. Okazaki, M., Ohmae, H., Takahashi, J., Kimura, H., and Sakuda, M. Insolubilized properties of UV-irradiated CO_3 apatite-collagen composites. Biomaterials **11**, 568, 1990.
12. Kikuchi, M., Itoh, S., Ichinose, S., Shinomiya, K., and Tanaka, J. Self-organization mechanism in a bone-like hydroxyapatite/collagen nanocomposite synthesized in vitro and its biological reaction in vivo. Biomaterials **22**, 1705, 2001.
13. Brown, W.E., Smith, J.P., Lehr, J.R., and Frazier, A.W.. Crystallographic and chemical relations between octacalcium phosphate and hydroxyapatite. Nature **196**, 1050, 1962.
14. Bohner, M. Resorbable biomaterials as bone graft substitutes. Materials Today **13**, 24, 2010.
15. Suzuki, O., Imaizumi, H., Kamakura, S., and Katagiri, T. Bone regeneration by synthetic octacalcium phosphate and its role in biological mineralization. Curr Med Chem **15**, 305, 2008.
16. Takami, M., Mochizuki, A., Yamada, A., Tachi, K., Zhao, B., Miyamoto, Y., Anada, T., Honda, Y., Nakamura, M., Suzuki, O., and Kamijo, R. Osteoclast differentiation induced by synthetic octacalcium phosphate through RANKL expression in osteoblasts. Tissue Eng Part A **15**, 3991, 2009.
17. Anada, T., Kumagai, T., Honda, Y., Masuda, T., Kamijo, R., Kamakura, S., Yoshihara, N., Kuriyagawa, T., Shimauchi, H., and Suzuki, O. Dose-dependent osteogenic effect of octacalcium phosphate on mouse bone marrow stromal cells. Tissue Eng **14**, 965, 2008.
18. Shelton, R.M., Liu, Y., Cooper, P.R., Gbureck, U., German, M.J., and Barralet, J.E. Bone marrow cell gene expression and tissue construct assembly using octacalcium phosphate microscaffolds. Biomaterials **27**, 2874, 2006.
19. Suzuki, O., Kamakura, S., Katagiri, T., Nakamura, M., Zhao, B., Honda, Y., and Kamijo, R. Bone formation enhanced implanted octacalcium phosphate involving conversion into Ca-deficient hydroxyapatite. Biomaterials **27**, 2671, 2006.
20. Kamakura, S., Sasano, Y., Shimizu, T., Hatori, K., Suzuki, O., Kagayama, M., and Motegi, K. Implanted octacalcium phsphate is more resorbable than beta-tricalcium phosphate and hydroxyapatite. J Biomed Mater Res **59**, 29, 2002.
21. Miyatake, N., Kishimoto, K.N., Anada, T., Imaizumi, H., Itoi, E., and Suzuki, O. Effect of partial hydrolysis of octacalcium phosphate on its osteoconductive characteristics. Biomaterials **30**, 1005, 2009.
22. Suzuki, O., Nakamura, M., Miyasaka, Y., Kagayama, M., and Sakurai, M. Bone formation on synthetic precursors of hydroxyapatite. Tohoku J Exp Med **164**, 37, 1991.
23. Kamakura, S., Sasaki, K., Honda, Y., Anada, T., and Suzuki, O. Octacalcium phosphate combined with collagen orthotopically enhances bone regeneration. J Biomed Mater Res B Appl Biomater **79**, 210, 2006.
24. Fuji, T., Anada, T., Honda, Y., Shiwaku, Y., Koike, H., Kamakura, S., Sasaki, K., and Suzuki, O. Octacalcium phosphate-precipitated alginate scaffold for bone regeneration. Tissue Eng Part A **15**, 3525, 2009.
25. Williams, D.F. On the mechanisms of biocompatibility. Biomaterials **29**, 2941, 2008.
26. Rezwan, K., Chen, Q.Z., Blaker, J.J., and Boccaccini, A.R. Biodegradable and bioactive porous polymer/inorganic composite scaffolds for bone tissue engineering. Biomaterials **27**, 3413, 2006.
27. Bonfield, W. Designing porous scaffolds for tissue engineering. Philos Transact A Math Phys Eng Sci **364**, 227, 2006.
28. Murakami, Y., Honda, Y., Anada, T., Shimauchi, H., and Suzuki, O. Comparative study on bone regeneration by synthetic octacalcium phosphate with various granule sizes. Acta Biomater **6**, 1542, 2010.
29. Kawai, T., Anada, T., Honda, Y., Kamakura, S., Matsui, K., Matsui, A., Sasaki, K., Morimoto, S., Echigo, E., and Suzuki, O. Synthetic octacalcium phosphate augments bone regeneration correlated with its content in collagen scaffold. Tissue Eng Part A **15**, 23, 2009.
30. Suzuki, O., Nakamura, M., Miyasaka, Y., Kagayama, M., and Sakurai, M. Maclura pomifera agglutinin-binding glycoconjugates on converted apatite from synthetic octacalcium phosphate implanted into subperiosteal region of mouse calvaria. Bone Miner **20**, 151, 1993.
31. Suzuki, O., Yagishita, H., Amano, T., and Aoba, T. Reversible structural changes of octacalcium phosphate and labile acid phosphate. J Dent Res **74**, 1764, 1995.
32. Fowler, B.O., Moreno, E.C., and Brown, W.E. Infra-red spectra of hydroxyapatite, octacalcium phosphate and pyrolysed octacalcium phosphate. Arch Oral Biol **11**, 477, 1966.
33. Nelson, D.G., and McLean, J.D. High-resolution electron microscopy of octacalcium phosphate and its hydrolysis products. Calcif Tissue Int **36**, 219, 1984.
34. Aoba, T., and Moreno, E.C. The enamel fluid in the early secretory stage of porcine amelogenesis: chemical composition and saturation with respect to enamel mineral. Calcif Tissue Int **41**, 86, 1987.
35. Moreno, E.C., and Aoba, T. Calcium bonding in enamel fluid and driving force for enamel mineralization in the secretory stage of amelogenesis. Adv Dent Res **1**, 245, 1987.
36. Moreno, E.C., and Aoba, T. Comparative solubility study of human dental enamel, dentin, and hydroxyapatite. Calcif Tissue Int **49**, 6, 1991.
37. Moreno, E.C., Kresak, M., and Zahradnik, R.T. Physicochemical aspects of fluoride-apatite systems relevant to the study of dental caries. Caries Res **11 Suppl 1**, 142, 1977.
38. Moreno, E.C., Brown, W.E., and Osborn, G. Stability of dicalcium phosphate dehydrate in aqueous solutions and solubility product of octacalcim phosphate. Soil Sci Soc Am Proc **24**, 99, 1960.
39. Mathew, M., Brown, W.E., Schroeder, L.W., and Dickens, B. Crystal structure of octacalcium bis(hydrogenphosphate) tetrakis(phosphate)pentahydrate, $Ca_8(HPO_4)_2(PO_4)_4 \cdot 5H_2O$. J Crystallogr Spectrosc Res **18**, 235, 1988.
40. Kamakura, S., Sasaki, K., Honda, Y., Anada, T., Matsui, K., Echigo, S., and Suzuki, O. Dehydrothermal treatment of collagen influences on bone regeneration by octacalcium phosphate (OCP) collagen composites. J Tissue Eng Regen Med **1**, 450, 2007.
41. Wang, M.C., Pins, G.D., and Silver, F.H. Collagen fibres with improved strength for the repair of soft tissue injuries. Biomaterials **15**, 507, 1994.
42. Weadock, K.S., Miller, E.J., Bellincampi, L.D., Zawadsky, J.P., and Dunn, M.G. Physical crosslinking of collagen fibers: comparison of ultraviolet irradiation and dehydrothermal treatment. J Biomed Mater Res **29**, 1373, 1995.
43. Kamakura, S., Sasano, Y., Homma, H., Suzuki, O., Kagayama, M., and Motegi, K. Implantation of octacalcium phosphate (OCP) in rat skull defects enhances bone repair. J Dent Res **78**, 1682, 1999.
44. Geiger, M., Li, R.H., and Friess, W. Collagen sponges for bone regeneration with rhBMP-2. Adv Drug Deliv Rev **55**, 1613, 2003.
45. Suzuki, O., Kamakura, S., and Katagiri, T. Surface chemistry and biological responses to synthetic octacalcium phosphate. J Biomed Mater Res Appl Biomater **77B**, 201, 2006.
46. Liu, Y., Cooper, P.R., Barralet, J.E., and Shelton, R.M. Influence of calcium phosphate crystal assemblies on the

proliferation and osteogenic gene expression of rat bone marrow stromal cells. Biomaterials **28**, 1393, 2007.
47. Imaizumi, H., Sakurai, M., Kashimoto, O., Kikawa, T., and Suzuki, O. Comparative study on osteoconductivity by synthetic octacalcium phosphate and sinterd hydroxyapatite in rabbit bone marrow. Calcif Tissue Int **78**, 45, 2006.
48. Honda, Y., Anada, T., Kamakura, S., Morimoto, S., Kuriyagawa, T., and Suzuki, O. The effect of microstructure of octacalcium phosphate on the bone regenerative property. Tissue Eng Part A **15**, 1965, 2009.
49. Oonishi, H., Hench, L.L., Wilson, J., Sugihara, F., Tsuji, E., Kushitani, S., and Iwaki, H. Comparative bone growth behavior in granules of bioceramic materials of various sizes. J Biomed Mater Res **44**, 31, 1999.
50. Sun, J.-S., Tsuang, Y.-H., Chang, W.H.-S., Li, J., Liu, H.-C., and Lin, F.-H. Effect of hydroxyapatite particle size on myoblasts and fibroblasts. Biomaterials **18**, 683, 1997.
51. Liu, H., Yazici, H., Ergun, C., Webster, T.J., and Bermek, H. An in vitro evaluation of the Ca/P ratio for the cytocompatibility of nano-to-micron particulate calcium phosphates for bone regeneration. Acta Biomater **4**, 1472, 2008.
52. Kikawa, T., Kahimoto, O., Imaizumi, H., Kokubun, S., and Suzuki, O. Intramembranous bone tissue response to biodegradable octacalcium phosphate implant. Acta Biomater **5**, 1756, 2009.
53. Suzuki, Y., Kamakura, S., Honda, Y., Anada, T., Hatori, K., Sasaki, K., and Suzuki, O. Appositional bone formation by OCP-collagen composite. J Dent Res **88**, 1107, 2009.
54. Brown, W.E. Crystal growth of bone mineral. Clin Orthop Rel Res **44**, 205, 1966.
55. Simpson, D.R. Problems of the composition and structure of the bone minerals. Clin Orthop Rel Res **86**, 260, 1972.
56. Young, R.A. Implications of atomic substitutions and other structural details in apatites. J Dent Res **53**, 193, 1974.
57. Doi, Y., Iwanaga, H., Shibutani, T., Moriwaki, Y., and Iwayama, Y. Osteoclastic responses to various calcium phosphates in cell cultures. J Biomed Mater Res **47**, 424, 1999.
58. Spence, G., Patel, N., Brooks, R., Bonfield, W., and Rushton, N. Osteoclastogenesis on hydroxyapatite ceramics: The effect of carbonate substitution. J Biomed Mater Res Part A **92A**, 1292, 2010.
59. Matsui, A., Anada, T., Masuda, T., Honda, Y., Miyatake, N., Kawai, T., Kamakura, S., Echigo, S., and Suzuki, O. Mechanical stress-related calvaria bone augmentation by onlayed octacalcium phosphate-collagen implant. Tissue Eng Part A **16**, 139, 2010.

Address correspondence to:
Osamu Suzuki, Ph.D., M.Eng.
Division of Craniofacial Function Engineering
Tohoku University Graduate School of Dentistry
4-1 Seiryo-machi
Aoba-ku, Sendai 980-8575
Japan

E-mail: suzuki-o@m.tohoku.ac.jp

Received: June 19, 2011
Accepted: September 21, 2011
Online Publication Date: October 31, 2011

NeuroImage 59 (2012) 1037–1042

Contents lists available at SciVerse ScienceDirect

NeuroImage

journal homepage: www.elsevier.com/locate/ynimg

Contralateral white noise attenuates 40-Hz auditory steady-state fields but not N100m in auditory evoked fields

Tetsuaki Kawase [a,b,c,*], Atsuko Maki [c], Akitake Kanno [d,e], Nobukazu Nakasato [f,g], Mika Sato [c], Toshimitsu Kobayashi [c]

[a] Laboratory of Rehabilitative Auditory Science, Tohoku University Graduate School of Biomedical Engineering, 6-6 Aoba, Aramaki, Aoba-ku, Sendai 980-8579, Japan
[b] Department of Audiology, Tohoku University Graduate School of Medicine, 1-1 Seiryo-machi, Aoba-ku, Sendai 980-8574, Japan
[c] Department of Otolaryngology-Head and Neck Surgery, Tohoku University Graduate School of Medicine, Sendai 980-8574, Japan
[d] Department of Functional Brain Imaging, Institute of Development, Aging and Cancer, Tohoku University, 4-1 Seiryo-cho, Aoba-ku, Sendai 980-8575, Japan
[e] MEG Laboratory, Kohnan Hospital, 4-20-1 Nagamachi-minami, Taihaku-ku, Sendai 982-8523, Japan
[f] Department of Epileptology, Tohoku University Graduate School of Medicine, Sendai 980-8574, Japan
[g] Department of Electromagnetic Neurophysiology, Smart Aging International Research Center, Institute of Development, Aging and Cancer, Tohoku University, Sendai 980-8575, Japan

ARTICLE INFO

Article history:
Received 22 May 2011
Revised 28 August 2011
Accepted 29 August 2011
Available online 14 September 2011

Keywords:
Magnetoencephalography
Auditory steady state response
Contralateral noise
Masking
40 Hz

ABSTRACT

The different response characteristics of the different auditory cortical responses under conventional central masking conditions were examined by comparing the effects of contralateral white noise on the cortical component of 40-Hz auditory steady state fields (ASSFs) and the N100m component in auditory evoked fields (AEFs) for tone bursts using a helmet-shaped magnetoencephalography system in 8 healthy volunteers (7 males, mean age 32.6 years). The ASSFs were elicited by monaural 1000 Hz amplitude modulation tones at 80 dB SPL, with the amplitude modulated at 39 Hz. The AEFs were elicited by monaural 1000 Hz tone bursts of 60 ms duration (rise and fall times of 10 ms, plateau time of 40 ms) at 80 dB SPL. The results indicated that continuous white noise at 70 dB SPL presented to the contralateral ear did not suppress the N100m response in either hemisphere, but significantly reduced the amplitude of the 40-Hz ASSF in both hemispheres with asymmetry in that suppression of the 40-Hz ASSF was greater in the right hemisphere. Different effects of contralateral white noise on these two responses may reflect different functional auditory processes in the cortices.

Introduction

Auditory masking is a phenomenon in which the audibility of one sound (signal) is decreased by the presence of another sound (masker). Under such masking conditions, the sensation thresholds for the signal sound are elevated and the amplitudes of the auditory evoked responses to the signal sound are usually reduced (Burkard and Sims, 2001; Dallos and Cheatham, 1976; Delgutte, 1996; Okamoto et al., 2005; Zwislocki, 1972, 1978). Understanding of the masking characteristics is important, since the signal is usually perceived in the presence of sounds other than signals in daily life. "Masking" is known to occur at any level of the auditory pathway from the cochlea to the cortex (Burkard and Sims, 2001; Dallos and Cheatham, 1976; Delgutte, 1996; Okamoto et al., 2005; Zwislocki, 1972, 1978), and is caused not only by sound presented to the ipsilateral ear but also by sound presented to the contralateral ear (Delgutte, 1996; Zwislocki, 1978). The major difference between ipsilateral and contralateral masking is the presence and absence, respectively, of direct interaction between signal stimuli and masking at the cochlear level. The effects of ipsilateral masking are usually much larger than those of contralateral masking, so the effects of peripheral masking, which occurs in the cochlea or cochlear nerve, are believed to be important in the ipsilateral masking phenomenon (Zwislocki, 1972, 1978). On the other hand, the contralateral masking phenomenon is often referred to as central masking, because the effect occurs between the ears; i.e., the brain is involved in the contralateral masking (Zwislocki, 1972, 1978).

One possible method to investigate central masking is to examine the contralateral masking phenomenon observed in auditory cortical evoked responses such as the N100 and 40-Hz auditory steady state responses (ASSRs), but the masking effects observed in evoked responses appear to be very different depending on the combinations of signal and masker properties (Bertoli et al., 2005; Galambos and Makeig 1992a, 1992b; Hari and Mäkelä, 1988; Maki et al., 2009; Okamoto et al., 2007) and possibly different between the right and left hemispheres (Okamoto et al., 2007).

* Corresponding author at: Laboratory of Rehabilitative Auditory Science, Tohoku University Graduate School of Medicine, 1-1 Seiryo-machi, Aoba-ku, Sendai 980-8574, Japan. Fax: +81 22 717 7307.
E-mail address: kawase@orl.med.tohoku.ac.jp (T. Kawase).

1053-8119/$ – see front matter © 2011 Elsevier Inc. All rights reserved.
doi:10.1016/j.neuroimage.2011.08.108

The N100 response, which is a prominent cortical response to transient auditory stimuli such as tone burst, is not significantly affected by contralateral continuous white noise (Hari and Mäkelä, 1988) or speech babble noise (Bertoli et al., 2005), but is significantly suppressed by speech sound, music sound, intermittent noise, and comb-filtered noise (Hari and Mäkelä, 1988; Okamoto et al., 2007). In contrast, any type of contralateral stimuli can suppress the 40-Hz ASSR, which is an oscillatory activity of the brain phase locked to the rhythm of the auditory stimulus such as repetition click, amplitude modulated (AM), and frequency modulated tones (Fujiki et al., 2002; Galambos and Makeig, 1992a, 1992b; Kaneko et al., 2003; Maki et al., 2009; Okamoto et al., 2007; Ross et al., 2005a). Considering the possible different effects of contralateral noise among the different types of contralateral sound, and the possible different effects depending on the observed condition such as stimulation ear and observed hemisphere, direct comparison between the different cortical evoked responses using the same contralateral sound is important. However, such a study has been conducted only for relatively complex noise (comb-filtered noise) (Okamoto et al., 2007), not for white noise, a basic type of contralateral noise. Moreover, the effects of contralateral white noise on the 40-Hz ASSR have not received detailed analysis including the hemispheric differences using magnetoencephalography (MEG), although several studies used electroencephalography (EEG) (Galambos and Makeig, 1992a, 1992b; Maki et al., 2009).

The present study compared the effects of contralateral white noise on the 40-Hz ASSR with the effects on the N100m using MEG, which can separate the activation of the auditory cortices in the right and left hemispheres (Hari et al., 1980; Kanno et al., 1996, 2000; Näätänen and Picton, 1987; Nakasato et al., 1995, 1997; Pantev et al., 1986, 1990; Reite et al., 1994), to examine whether the same contralateral white noise has different masking effects on the 40-Hz ASSR and N100m, and the possible different effects of contralateral white noise according to the simulation ear and/or observed hemisphere. Clarification of differences in the contralateral sound effects between the different evoked responses will help to elucidate the mechanisms of central masking and the generation mechanism of each evoked response.

Materials and methods

Subjects

This study included 8 normal volunteers (7 males and 1 female, mean +/− SD age of 32.6 +/− 8.63 years) without histories of auditory diseases or neurological disorders. All subjects were right-handed with scores above +90 on the Edinburgh Handedness Inventory (Oldfield, 1971). The present study was approved by the ethical committee of the Tohoku University Graduate School of Medicine and Kohnan Hospital. All parts of the present study were performed in accordance with the guidelines of the Declaration of Helsinki.

Stimuli

The stimulus to elicit the 40-Hz ASSR was a 1000-Hz continuous tone 100% AM at 39 Hz with an exponential modulation envelope (John et al., 2002), generated by a digital signal processing platform (TDT System III; Tucker-Davis Technologies, Gainesville, FL) under the control of an IBM PC/AT computer. The modulation of 39 Hz was chosen based on the preliminary measurement of two subjects in whom ASSRs in response to 39 Hz tended to be larger than those to 40 Hz, and the previous finding that the largest amplitude of ASSR is obtained at a frequency just below 40 Hz (Pastor et al., 2002). The sound pressure level of the AM tone was 80 dB SPL and presented monaurally.

The stimulus to elicit the N100m response was a tone burst of 60 ms duration (rise and fall times of 10 ms, plateau time of 40 ms) at a frequency of 1 kHz and presented monaurally. The sound pressure level of the tone burst was 80 dB SPL. The mean interstimulus interval was 3.33 s (0.3 Hz) with 50% interstimulus variance.

Continuous white noise at 70 dB SPL, which was almost the same noise level as our previous study (Maki et al., 2009), was applied as contralateral noise. Schematic drawings of the test protocols are presented in Fig. 1. The signals (AM tone and tone bursts) and noise were presented to the subject through a tube earphone (ER-3A; Etymotic Research, Elk Grove Village, IL; tube length, 1.5 m).

Recording

Auditory evoked fields (AEFs) were recorded in a magnetically shielded room using a 160-channel whole-head type axial gradiometer system (MEGvision PQ1160C; Yokogawa Electric, Musashino, Tokyo, Japan). Sensors are configured as first-order axial gradiometers with a baseline of 50 mm; each coil of the gradiometers measures 15.5 mm in diameter. The sensors are arranged in a uniform array on a helmet-shaped surface at the bottom of the dewar vessel, and the mean distance between the centers of two adjacent coils is 25 mm. The field sensitivities of the sensors (noise of the system) were 3 fT/Hz within the frequency range.

The AEFs were recorded only in the wake state as confirmed by real time monitoring of the occipital alpha rhythm by MEG. Subjects were instructed to keep awake during recording. If the subjects appeared to be sleepy, a break was taken to ameliorate the drowsiness of the subjects by conversation and/or by a short nap.

To obtain ASSRs, MEG signal was band-pass filtered between 0.03 Hz and 500 Hz and sampled at 2000 Hz. MEG signals during the presentation of continuous AM tone were recorded serially for 240 s, and the responses were analyzed afterward (offline). Data epochs of 4-s duration, starting at the onset of the trigger signal synchronized with a certain phase of the amplitude modulation, were cut off from the serial recorded data after filtering with digital band-pass filter (35–45 Hz) and averaged in the time domain.

To obtain the N100m response to tone bursts, the data from 100 ms before to 500 ms after the stimulus onset were averaged for 300 s (about 100 times). In the following off-line analysis, the averaged data were digitally band-pass filtered from 3.0 to 40.0 Hz. The N100m response was visually identified as the first prominent peak at 80–100 ms after the onset, with the isofield map confirming downward current orientation.

For both auditory steady state field (ASSF) and N100m responses, the location of each signal source was estimated using an equivalent current dipole model with the best fit sphere for each subject's head. The estimated source was superimposed on the three-dimensional magnetic resonance (MR) image of the individual subject using a MEG-MR image coordination integration system, to verify that the measured responses originated from the auditory cortex.

Measurement and analysis

ASSFs (or N100ms) in response to the AM tone without contralateral noise and with contralateral noise were measured alternately 3 times (Fig. 1). All data obtained from the measurements were used for the subsequent analysis. The starting condition (noise (+) or noise (−)) was randomized. Usually each participant started with the measurements of ASSFs in response to right ear stimulation with and without contralateral noise, then with the left ear, followed by N100m measurements in the right and left ears. ASSFs in response to stimulation of the right and left ears were always conducted in the same day, but N100m measurements in the right and left ears were examined on another day, considering the fatigue of the

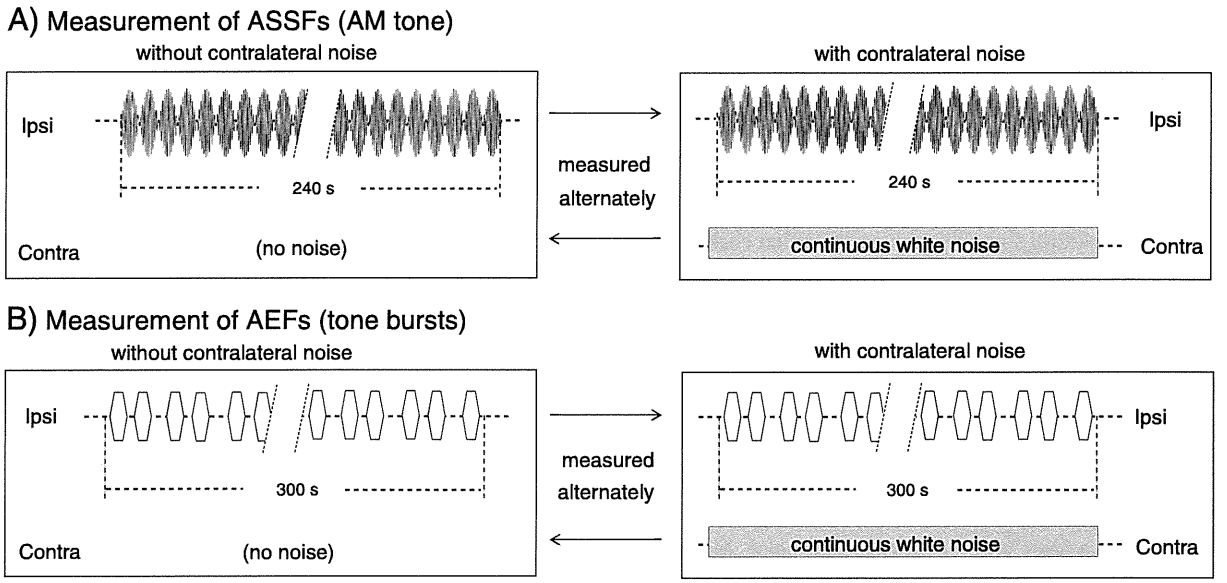

Fig. 1. Schematic drawing of the experimental protocols. (A) To elicit the ASSF, 39-Hz AM tone at 1000 Hz (80 dB SPL) was continuously presented monaurally for 240 s, with or without contralateral continuous white noise (70 dB SPL). (B) To elicit the N100m response, tone bursts of 60 ms duration (rise and fall times of 10 ms, plateau time of 40 ms) at a frequency of 1000 Hz (80 dB SPL) was presented monaurally for 300 s (mean interstimulus interval was 3.33 s with 50% interstimulus variance), with or without contralateral continuous white noise (70 dB SPL). ASSFs (or N100m) in response to AM tone (or tone bursts) without contralateral noise and those with contralateral noise were measured alternately 3 times. (See text for further details.).

subjects. Basically, all subjects were expected to participate in all four measurements.

In the present study, the effects of contralateral noise on the amplitudes of ASSFs and N100m were analyzed by focusing on the channels with the maximum signals measured over each hemisphere. The amplitude of the ASSF at the channels with the maximum signal of each hemisphere was assessed by fast Fourier transform at 1000 ms after the onset of the AM tone. On the other hand, the amplitude of the N100m at the channels with the maximum signal of each hemisphere was determined as a peak amplitude (baseline to peak) of the averaged response.

The measured amplitudes obtained under the same conditions of signal and contralateral noise (actually three values for each sound condition) were averaged, and the effects of contralateral noise on the ASSFs or N100m were analyzed in the right and left hemispheres.

Results

ASSFs were observed in the bilateral hemispheres of all subjects, under all four stimulus conditions; i.e., right and left ear stimulations with/without contralateral noise. On the other hand, the N100ms in response to tone bursts were recorded in 15 ears of 8 subjects (N100m was not measured accidentally in the left ear of one subject). However, no apparent N100m was obtained in two subjects in either or both hemispheres in response to stimulation of one or both ears by recurrent measurements, despite normal hearing thresholds and positive ASSFs. As a result, the effects of contralateral noise on the N100m in response to right ear stimulation were assessed in 7 right and 7 left hemispheres, and in response to left ear stimulation in 7 right and 5 left hemispheres. This data set for N100m was inappropriate for statistical analysis using analysis of variance (ANOVA), because not all of the seven or five subjects were the same in each measurement condition, so this dataset could be paired up only with and without contralateral noise in every measurement condition. Consequently, the paired *t*-test was used for analysis of the N100m data. On the other hand, repeated measures ANOVA was applied for the statistical analysis of the ASSR data.

Figs. 2A and 3A show examples of the effects of contralateral noise on the ASSFs and N100m waveform, respectively, arranged in a flattened projection of the sensor position. Figs. 2B, C, 3B, and C illustrate the waveforms at the sensors with the largest amplitude in each hemisphere. In both cases, the stimulus and masker were presented to the right and left ears, respectively. Suppression of the ASSFs caused by the contralateral noise was observed in the bilateral hemispheres, but the magnitude of suppression appeared to be larger in the right hemisphere than in the left hemisphere, whereas no apparent suppression of N100m was observed.

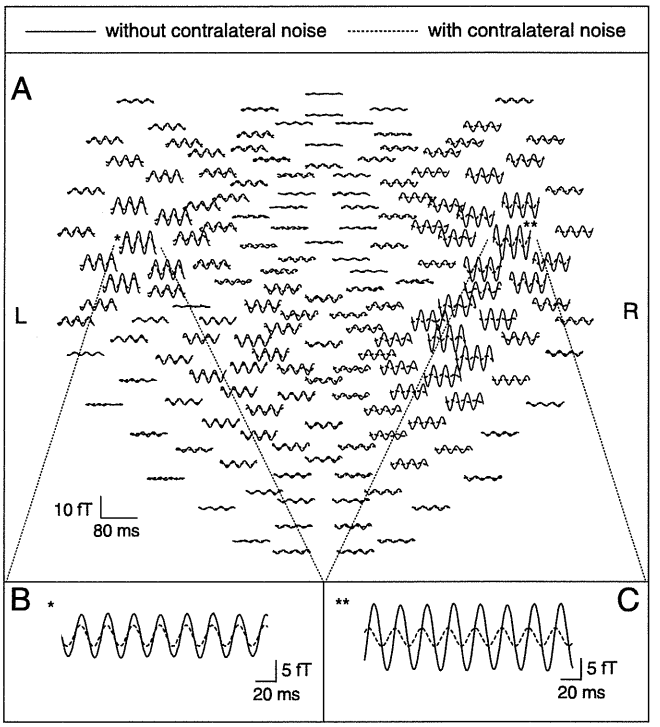

Fig. 2. Example of effects of contralateral noise on the waveform of ASSF (Case KH, right ear stimulation of AM signal). (A) Waveforms of ASSF with contralateral noise are superimposed on waveforms without contralateral noise, arranged in a flattened projection of the sensor position. (B and C) ASSF waveforms at the sensors with the largest amplitude of ASSF in each hemisphere.

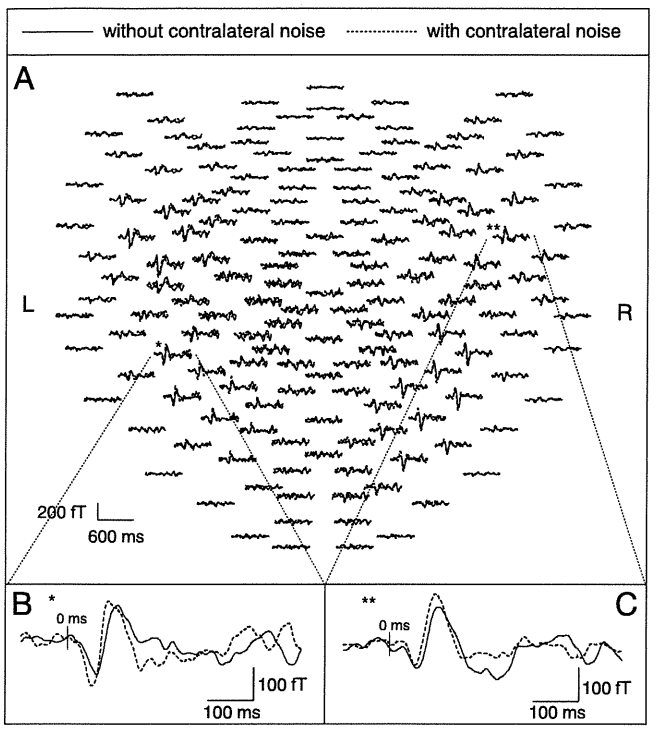

Fig. 3. Example of effects of contralateral noise on the waveform of N100m (Case YH, right ear stimulation of tone bursts). (A) Waveforms of N100m with contralateral noise are superimposed on waveforms without contralateral noise, arranged in a flattened projection of the sensor position. (B and C) N100m waveforms at the sensors with the largest amplitude of N100m in each hemisphere.

Figs. 4A and B show the averaged effects of contralateral noise on the amplitudes of ASSFs and N100m in the channels of the maximum signals measured over each hemisphere for all measurement conditions. Statistical analyses of the ASSF data were performed using three-way repeated measures ANOVA, with the within-subject factors of stimulated side of the ear (stimulation; right/left), measured side of the hemisphere (hemisphere; right/left), and the presence of contralateral noise (noise; off/on). For the maximum amplitude of the ASSF, the main effects of hemisphere ($F(1,7)=12.75$, $p=0.0091$) and noise ($F(1,7)=21.79$, $p=0.0023$) were significant, but the main effect of stimulation was not significant ($F(1,7)=0.18$, $p=0.68$). There were significant first-order interactions between stimulation and noise ($F(1,7)=7.21$, $p=0.031$), between hemisphere and noise ($F(1,7)=9.36$, $p=0.0183$), and between hemisphere and stimulation ($F(1,7)=7.48$, $p=0.029$). The second-order interaction was not significant ($F(1,7)=2.21$, $p=0.18$). The simple main effect of noise was significant for both stimulations ($F(1,7)=34.23$, $p=0.0006$ for the right ear stimulation and $F(1,7)=8.20$, $p=0.024$ for the left), and both hemispheres ($F(1,7)=28.02$, $p=0.0011$ for the right hemisphere and $F(1,7)=6.42$, $p=0.039$ for the left), indicating that contralateral noise significantly suppressed the ASSRs of both hemispheres regardless of the side of stimulation. The simple main effect of hemisphere was also significant for both noise conditions ($F(1,7)=14.69$, $p=0.0064$ without contralateral noise and $F(1,7)=9.31$, $p=0.019$ with contralateral noise), indicating that the maximum ASSR amplitude was significantly higher in the right hemisphere than in the left regardless of the presence of contralateral noise. The simple main effect of stimulation of the left hemisphere ($F(1,7)=8.09$, $p=0.025$) and the simple main effect of hemisphere for left ear stimulation ($F(1,7)=11.22$, $p=0.012$) were both significant. In contrast, the same contralateral noise had no significant effects on the amplitude of N100m for all measurement conditions (Fig. 4B, paired t-test).

Fig. 5 shows the suppression magnitude expressed as the ratio of ASSF amplitudes observed with and without contralateral noise. The data was analyzed by two-way repeated measures ANOVA, with the within-subject factors of stimulated side of the ear (stimulation; right/left), and measured side of the hemisphere (hemisphere; right/left). The main effect of the hemisphere was significant ($F(1,7=8.00$, $p=0.0026$), indicating the suppression magnitude induced by the contralateral noise was significantly greater in the right hemisphere than in the left. The main effect of stimulation ($F(1,7)=3.21$, $p=0.12$) and the interaction ($F(1,7)=1.85$, $p=0.22$) were not significant.

Discussion

The present study compared the contralateral noise effect between the cortical component of the 40-Hz ASSF and the N100m component of the AEFs for tone bursts. The results clearly showed that continuous white noise at 70 dB SPL presented to the contralateral ear did not suppress the N100m response in either hemisphere, but significantly reduced the amplitude of the 40-Hz ASSF in both hemispheres, with the hemispheric asymmetry that suppression of the 40-Hz ASSF was significantly greater in the right hemisphere. This possible differential masking effect of contralateral sound between the N100m and 40-Hz ASSF may be an important observation reflecting the different

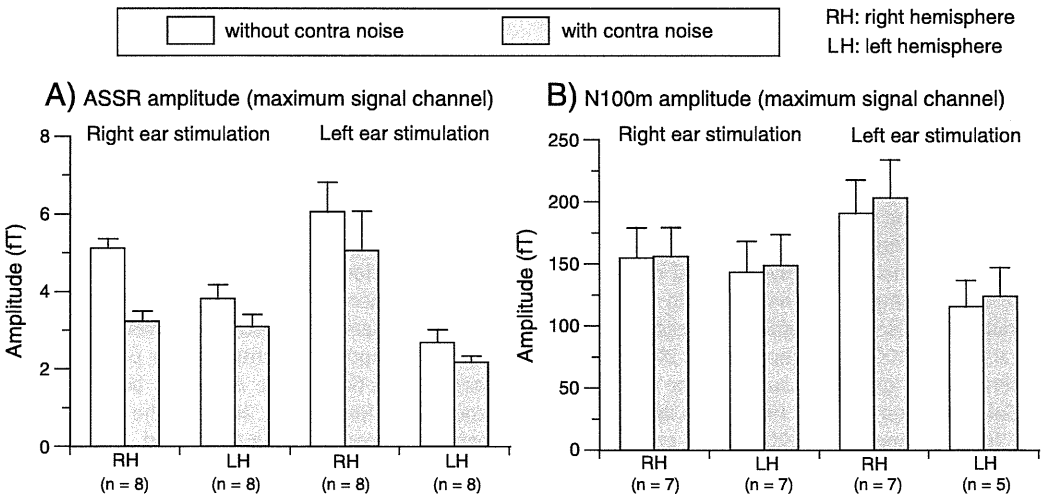

Fig. 4. Averaged effects of contralateral noise on the amplitudes of ASSFs and N100m at the channels of maximum signals measured over each hemisphere (A and B) (see text for further details).

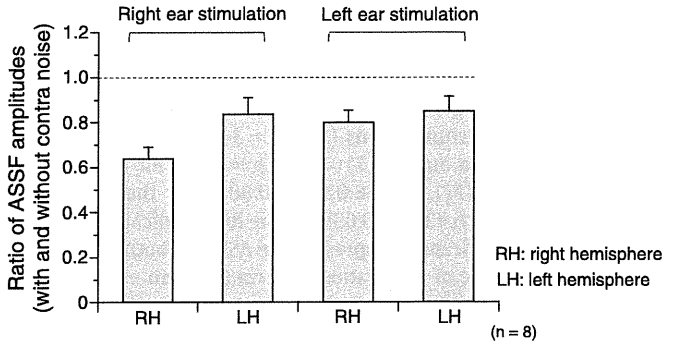

Fig. 5. Suppression magnitudes expressed as the ratio of ASSF amplitudes observed with and without contralateral noise (see text for further details).

functional roles of these two cortical responses in auditory processing of the cortices.

Differential contralateral effects on different auditory evoked responses

Direct comparison between the effects of contralateral continuous broadband noise on the 40-Hz ASSR and the findings of other auditory tests, such as psychophysical measurements and evoked responses like auditory brainstem response (ABR) and 80-Hz ASSR, has suggested that the 40-Hz ASSR is suppressed by contralateral noise without significant change in the psychophysical threshold, ABR, and 80-Hz ASSR (Galambos and Makeig, 1992a, 1992b; Maki et al., 2009). Since the ABR and the major part of the 80-Hz ASSR recorded by EEG are thought to originate from the brainstem (Aoyagi et al., 1999; Herdman et al., 2002; Kuwada et al., 1986; Picton et al., 2003; Ross et al., 2000; Wong and Stapells, 2004), the upper auditory pathway as the auditory cortex may be mainly responsible for suppression of the 40-Hz ASSR by contralateral noise (Galambos and Makeig, 1992a, 1992b; Maki et al., 2009).

On the other hand, the present study showed that the 40-Hz ASSR is suppressed by contralateral continuous white noise without significant change of the N100m response; i.e., although both 40-Hz ASSR and N100m are auditory cortical responses, there was a difference in the binaural phenomenon. N100m is an onset response to transient stimuli delivered as tone bursts, whereas the ASSR is an oscillatory activity of the brain, which is phase locked to the rhythm of the auditory stimulus. Moreover, source localization of the 40-Hz ASSR and N100m has shown that the 40-Hz ASSR sources are significantly separated from the N100m source in the auditory cortex (Engelien et al., 2000; Mäkelä and Hari, 1987; Okamoto et al., 2007; Pantev et al., 1996; Ross et al., 2005b). Therefore, the N100m and cortical ASSR probably reflect different functional processes in different locations in the auditory cortex. The different contralateral effects observed for the 40-Hz ASSR and N100m may be one aspect of such different functional processes.

On the other hand, our results were somewhat different from the previous study directly comparing contralateral noise effects between N100m and ASSR using the different complex stimuli such as pass-band or stop-band stimulus consisting of five spectral components and comb-filter noise as the contralateral noise; i.e., in their study, the addition of contralateral noise significantly suppressed not only the 40-Hz ASSR but also the N100m (Okamoto et al., 2007). So far, any type of contralateral sound appears to suppress the 40-Hz ASSR (Fujiki et al., 2002; Galambos and Makeig, 1992a, 1992b; Kaneko et al., 2003; Maki et al., 2009; Okamoto et al., 2007; Ross et al., 2005a). On the other hand, suppression of the N100m by contralateral noise appears to be very dependent on the type of contralateral noise (Bertoli et al., 2005; Hari and Mäkelä, 1988; Okamoto et al., 2007). Thus, the different results in our present study and Okamoto's study may simply reflect the latter factor concerning N100m. However, direct investigation of the phenomenon seems important to establish the differential effects of contralateral masking among the different types of responses originating from the auditory cortex.

The effects of contralateral white noise on N100m amplitude were not significant, but the average amplitudes of N100m were slightly larger with contralateral white noise than without contralateral noise under all measurement conditions, as shown in Fig. 4B. Interestingly, this finding was quite similar to those obtained in a study based on limited observing conditions using signal tone bursts and contralateral noise applied from the right and left ears, respectively, and N100m observed from the right hemisphere using 7 channel MEG (Hari and Mäkelä, 1988). Further study would be necessary to examine the possible existence of small enhancement effects of contralateral white noise on N100m.

Hemispheric asymmetry of contralateral suppression

The effects of contralateral white noise on the 40-Hz ASSR have been mainly examined by conventional EEG methods (Galambos and Makeig, 1992a, 1992b; Maki et al., 2009). The present results obtained by MEG showed evoked ASSRs can separate activation of the auditory cortex in the right and left hemispheres, and showed significant right hemispheric predominance in the suppression of the 40-Hz ASSF. The contralateral sound effects on 40-Hz ASSFs have been examined using several types of contralateral sound (Fujiki et al., 2002; Kaneko et al., 2003; Okamoto et al., 2007; Ross et al., 2005a), and the hemispheric differences in contralateral suppression appear to be somewhat different depending on the contralateral sound. No apparent hemispheric differences were observed using comb-filter noise as the contralateral noise (Okamoto et al., 2007). On the other hand, ASSFs evoked by the AM tones applied binaurally were more suppressed in the hemisphere ipsilateral to the stimulation ear (Kaneko et al., 2003). The apparent right hemispheric predominance in contralateral sound effects on 40-Hz ASSFs was only identified in the present study using white noise as the contralateral sound. The different hemispheric asymmetry according to the type of contralateral suppressor indicates that the suppression mechanism may not be exactly the same for various contralateral suppressors, although the ASSR is suppressed by any type of contralateral sound.

Hemispheric asymmetry observed in contralateral noise suppression may be explained by the right hemispheric predominance of ASSR (Ross et al., 2005b) and contralateral hemispheric predominance for simple noise stimuli (Schönwiesner et al., 2007). The right hemispheric predominance of ASSR, also found in the present study, possibly indicates the special role of the right auditory cortex in the generation of ASSR. The largest contralateral noise effect may be observed for this special process in the right hemisphere with noise presented to the left ear, or may simply reflect the left hemispheric predominance in signal processing under masking conditions as indicated by the observation of N100m (Okamoto et al., 2007).

Functional relevance of different contralateral noise effects

The functional significance of the 40-Hz ASSR, i.e. what kind of auditory processing or function is mediated by the 40-Hz ASSR, has not yet been fully clarified. However, the ASSRs appear to represent the temporal structure and/or periodicity of the sound, so the possible function of the ASSR has been assumed to involve pitch processing (Ross et al., 2005b). The right hemisphere dominance seen for the cortical ASSR (Ross et al., 2005b), as well as the possible important role of the right hemisphere for the perception of missing fundamentals (Zatorre, 1988), pitch discrimination for complex sound (Johnsrude et al., 2000), discrimination of the temporal structure of the sound (Samson and Zatorre, 1994), and other observations, is

thought to support this idea (Ross et al., 2005b). On the other hand, the relationship between the 40-Hz ASSR and the simple perception of the sound appears to be relatively poor, i.e., the change in ASSR is not closely related to the change in psychophysical threshold (Galambos and Makeig, 1992a, 1992b; Maki et al., 2009). A similar level of noise to that used in the present study caused no significant psychophysical threshold elevation, significant threshold elevation of the 40-Hz ASSR (average 10–15 dB), and no significant threshold elevation of the 80-Hz ASSR (Maki et al., 2009). Moreover, the change in the psychophysical threshold observed in the masking level difference phenomenon could not be observed in the 40-Hz ASSR (Ishida and Stapells, 2009), but was seen in the N100m (Sasaki et al., 2005). These discrepancies between psychophysical threshold change and 40-Hz ASSR may indicate that the 40-Hz ASSR does not directly reflect the neural process to detect psychophysical threshold sensation, whereas the N100m appears to be more related to the simple psychophysical perception of the sound. Therefore, the types of psychophysical percepts related to the 40-Hz ASSR have not been clarified, so the type of perceptual aspect of 40-Hz AM tone that is affected without threshold change by the contralateral noise requires investigation.

Conflicts of interest statement

The authors declare no conflicts of interest.

Acknowledgments

We wish to thank staff of Kohnan Hospital Ryogo Center for their continuous support of this work. We also thank Prof. Tsuji (Department of Public Health & Forensic Medicine, Tohoku University Graduate School of Medicine) for his helpful suggestion on the statistics of the data.

This study was supported by grant from the Ministry of Education, Culture, Sports, Science and Technology-Japan (Grant-in-Aid for Exploratory Research 15659401).

References

Aoyagi, M., Suzuki, Y., Yokota, M., Furuse, H., Watanabe, T., Ito, T., 1999. Reliability of 80-Hz amplitude-modulation-following response detected by phase coherence. Audiol. Neurootol. 4, 28–37.

Bertoli, S., Smurzynski, J., Probst, R., 2005. Effects of age, age-related hearing loss, and contralateral cafeteria noise on the discrimination of small frequency changes: psychoacoustic and electrophysiological measures. J. Assoc. Res. Otolaryngol. 6, 207–222.

Burkard, R.F., Sims, D., 2001. The human auditory brainstem response to high click rates: aging effects. Am. J. Audiol. 10, 53–61.

Dallos, P., Cheatham, M.A., 1976. Compound action potential (AP) tuning curves. J. Acoust. Soc. Am. 59, 591–597.

Delgutte, B., 1996. Physiological models for basic auditory percepts. In: Hawkins, H.L., McMullen, T.A., Popper, A.N., Fay, R.R. (Eds.), Auditory computation. Springer, New York, Berlin, Heidelberg, pp. 157–220.

Engelien, A., Schulz, M., Ross, B., Arolt, V., Pantev, C., 2000. A combined functional in vivo measure for primary and secondary auditory cortices. Hear. Res. 148, 153–160.

Fujiki, N., Jousmaki, V., Hari, R., 2002. Neuromagnetic responses to frequency-tagged sounds: a new method to follow inputs from each ear to the human auditory cortex during binaural hearing. J. Neurosci. 22, RC205.

Galambos, R., Makeig, S., 1992a. Physiological studies of central masking in man. I: The effects of noise on the 40-Hz steady-state response. J. Acoust. Soc. Am. 92, 2683–2690.

Galambos, R., Makeig, S., 1992b. Physiological studies of central masking in man. II: Tonepip SSRs and the masking level difference. J. Acoust. Soc. Am. 92, 2691–2697.

Hari, R., Mäkelä, J.P., 1988. Modification of neuromagnetic responses of the human auditory cortex by masking sounds. Exp. Brain Res. 71, 87–92.

Hari, R., Aittoniemi, K., Jarvinen, M.J., Katila, T., Varpula, T., 1980. Auditory evoked transient and sustained magnetic fields of the human brain: Localization of neural generators. Exp. Brain Res. 40, 237–240.

Herdman, A.T., Lins, O., Van Roon, P., Stapells, D.R., Scherg, M., Picton, T.W., 2002. Intracerebral sources of human auditory steady-state responses. Brain Topogr. 15, 69–86.

Ishida, I.M., Stapells, D.R., 2009. Does the 40-Hz auditory steady-state response show the binaural masking level difference? Ear Hear. 30, 713–715.

John, M.S., Dimitrijevic, A., Picton, T.W., 2002. Auditory steady-state responses to exponential modulation envelopes. Ear Hear. 23, 106–117.

Johnsrude, I.S., Penhune, V.B., Zatorre, R.J., 2000. Functional specificity in the right human auditory cortex for perceiving pitch direction. Brain 123, 155–163.

Kaneko, K., Fujiki, N., Hari, R., 2003. Binaural interaction in the human auditory cortex revealed by neuromagnetic frequency tagging: no effect of stimulus intensity. Hear. Res. 183, 1–6.

Kanno, A., Nakasato, N., Fujita, S., Seki, K., Kawamura, T., Ohtomo, S., Fujiwara, S., Yoshimoto, T., 1996. Right hemispheric dominance in the auditory evoked magnetic fields for pure-tone stimuli. Electroencephalogr. Clin. Neurophysiol. Suppl. 47, 129–132.

Kanno, A., Nakasato, N., Murayama, N., Yoshimoto, T., 2000. Middle and long latency peak sources in auditory evoked magnetic fields for tone bursts in humans. Neurosci. Lett. 293, 187–190.

Kuwada, S., Batra, R., Maher, V.L., 1986. Scalp potentials of normal and hearing-impaired subjects in response to sinusoidally amplitude-modulated tones. Hear. Res. 21, 179–192.

Mäkelä, J.P., Hari, R., 1987. Evidence for cortical origin of the 40 Hz auditory evoked response in man. Electroencephalogr. Clin. Neurophysiol. 66, 539–546.

Maki, A., Kawase, T., Kobayashi, T., 2009. Effects of contralateral noise on 40-Hz and 80-Hz auditory steady-state responses. Ear Hear. 30, 584–589.

Näätänen, R., Picton, T., 1987. The N1 wave of the human electric and magnetic response to sound: a review and an analysis of the component structure. Psychophysiology 24, 375–425.

Nakasato, N., Fujita, S., Seki, K., Kawamura, T., Matani, A., Tamura, I., Fujiwara, S., Yoshimoto, T., 1995. Functional localization of bilateral auditory cortices using an MRI-linked whole head magnetoencephalography (MEG) system. Electroencephalogr. Clin. Neurophysiol. 94, 183–190.

Nakasato, N., Kumabe, T., Kanno, A., Ohtomo, S., Mizoi, K., Yoshimoto, T., 1997. Neuromagnetic evaluation of cortical auditory function in patients with temporal lobe tumors. J. Neurosurg. 86, 610–618.

Okamoto, H., Kakigi, R., Gunji, A., Kubo, T., Pantev, C., 2005. The dependence of the auditory evoked N1m decrement on the bandwidth of preceding notch-filtered noise. Eur. J. Neurosci. 21, 1957–1961.

Okamoto, H., Stracke, H., Ross, B., Kakigi, R., Pantev, C., 2007. Left hemispheric dominance during auditory processing in a noisy environment. BMC Biol. 5, 52.

Oldfield, R.C., 1971. The assessment and analysis of handedness: the Edinburgh inventory. Neuropsychologia 9, 97–113.

Pantev, C., Lutkenhoner, B., Hoke, M., Lehnertz, K., 1986. Comparison between simultaneously recorded auditory-evoked magnetic fields and potentials elicited by ipsilateral, contralateral and binaural tone burst stimulation. Audiology 25, 54–61.

Pantev, C., Hoke, M., Lehnertz, K., Lutkenhoner, B., Fahrendorf, G., Stober, U., 1990. Identification of sources of brain neuronal activity with high spatiotemporal resolution (NMSL) and magnetic resonance imaging (MRI). Electroencephalogr. Clin. Neurophysiol. 75, 173–184.

Pantev, C., Roberts, L.E., Elbert, T., Ross, B., Wienbruch, C., 1996. Tonotopic organization of the sources of human auditory steady-state responses. Hear. Res. 101, 62–74.

Pastor, M.A., Artieda, J., Arbizu, J., Marti-Climent, J.M., Peñuelas, I., Masdeu, J.C., 2002. Activation of human cerebral and cerebellar cortex by auditory stimulation at 40 Hz. J. Neurosci. 22, 10501–10506.

Picton, T.W., John, M.S., Dimitrijevic, A., Purcell, D., 2003. Human auditory steady-state responses. Int. J. Audiol. 42, 177–219.

Reite, M., Adams, M., Simon, J., Teale, P., Sheeder, J., Richardoson, D., Grabbe, R., 1994. Auditory M100 component 1: relationship to Heschl's gyri. Cogn. Brain Res. 2, 13–20.

Ross, B., Borgmann, C., Draganova, R., Roberts, L.E., Pantev, C., 2000. A high-precision magnetoencephalographic study of human auditory steady-state responses to amplitude-modulated tones. J. Acoust. Soc. Am. 108, 679–691.

Ross, B., Herdman, A.T., Pantev, C., 2005a. Stimulus induced desynchronization of human auditory 40-Hz steady-state responses. J. Neurophysiol. 94, 4082–4093.

Ross, B., Herdman, A.T., Pantev, C., 2005b. Right hemispheric laterality of human 40 Hz auditory steady-state responses. Cereb. Cortex 15, 2029–2039.

Samson, S., Zatorre, R.J., 1994. Contribution of the right temporal lobe to musical timbre discrimination. Neuropsychologia 32, 231–240.

Sasaki, T., Kawase, T., Nakasato, N., Kanno, A., Ogura, M., Tominaga, T., Kobayashi, T., 2005. Neuromagnetic evaluation of binaural unmasking. Neuroimage 25, 684–689.

Schönwiesner, M., Krumbholz, K., Rübsamen, R., Fink, G.R., von Cramon, D.Y., 2007. Hemispheric asymmetry for auditory processing in the human auditory brain stem, thalamus, and cortex. Cereb. Cortex 17, 492–499.

Wong, W.Y.S., Stapells, D.R., 2004. Brain stem and cortical mechanisms underlying the binaural masking level difference in humans: an auditory steady-state response study. Ear Hear. 25, 57–67.

Zatorre, R.J., 1988. Pitch perception of complex tones and human temporal-lobe function. J. Acoust. Soc. Am. 84, 566–572.

Zwislocki, J.J., 1972. A theory of central auditory masking and its partial validation. J. Acoust. Soc. Am. 52, 644–659.

Zwislocki, J.J., 1978. Masking: Experimental and theoretical aspects of simultaneous, forward, backward, and central masking. In: Carterette, E.C., Friedman, M.P. (Eds.), Handbook of perception, volume IV, hearing. Academic Press, New York, San Francisco, London, pp. 283–336.

Gait & Posture xxx (2012) xxx–xxx

Contents lists available at SciVerse ScienceDirect

Gait & Posture

journal homepage: www.elsevier.com/locate/gaitpost

Influence of constrained visual and somatic senses on controlling centre of mass during sit-to-stand

Yuko Kuramatsu, Takayuki Muraki, Yutaka Oouchida, Yusuke Sekiguchi, Shin-Ichi Izumi *

Department of Physical Medicine and Rehabilitation, Tohoku University Graduate School of Medicine, Japan

ARTICLE INFO

Article history:
Received 16 August 2011
Received in revised form 3 December 2011
Accepted 15 January 2012

Keywords:
Perception–action coupling
Centre of mass
Sit-to-stand
Perceptual constraint
Postural orientation

ABSTRACT

This study aimed to investigate the manner in which healthy individuals execute robust whole body movements despite unstable body structure from the perspective of perception–action coupling. Twelve healthy adults performed sit-to-stand (STS) movements under conditions of constrained visual and somatic senses. During this movement, centre of mass (COM) of the body in the anterior–posterior, upward–downward and right–left directions was computed. The conditions of perceptual constraint were set as vision-restricted, somatosensory-restricted, vision- and somatosensory-restricted, and normal conditions. To evaluate COM control under these perceptual constraints, the variability in position and velocity of COM were assessed. The variabilities in COM velocity in the anterior–posterior and upward–downward directions decreased around the lift-off period only when both vision and somatic senses were constrained, whereas the variability of the COM position in the right–left direction increased under the somatosensory-restricted condition. Our findings suggested that control of COM velocity was enhanced in the major moving directions (anterior and upward directions) around the lift-off period during STS when both modalities of perception with regard to postural orientation were constrained. These motor regulations with perceptual constraints facilitate better adaptation to changes in body and environmental situations in daily life.

1. Introduction

Perception of postural orientation, which integrates and assesses afferent information from peripheral sensors, is essential for executing motor tasks [1]. With this perception, healthy individuals can perform daily activities unfailingly in different body and environmental situations despite an inherently unstable body structure [2]. Particularly, perception–action coupling is well coordinated during daily routine movements such as stepping to walk and grasping, which are well-practised and skilfully performed [3,4]. In contrast, patients with motor disorders frequently demonstrate inappropriate coordination between perception and action, which results in an inability to perform motor tasks even with minimal disturbance or minimally changing environmental situations [5–7]. Therefore, understanding perception–action coupling under conditions of perceptual constraints is important to improve performance of motor tasks and to treat patients with motor disorders.

Previous authors have investigated the relationship between static posture control and perception [8,9]. In addition, most previous studies on the relationship between perception and action have focused on focal movements of the restrained upper extremities in stable sitting positions [10,11], and not on whole-body movements performed during daily living activities. Whole-body dynamics have often been studied via a mechanical approach, such as analyses of joint motion at a physical level [12,13]. However, using the uncontrolled manifold (UCM) hypothesis, Reisman et al. analysed a dynamic whole-body movement under varying support surface conditions which influenced the mechanical and perceptual situation [14]. In the Bernstein problem [15], motor variability is organised such that important task-related variables are preferentially controlled by the nervous system. However, they focused on the mechanics of motor coordination to achieve the task goal rather than on the relationship between perception and action.

The close relationship between perception and action, particularly for postural orientation, is believed to transform the unstable structure into a controllable system [1]. Multiple modalities including visual, somatosensory, and vestibular systems are redundantly involved to perceive postural orientation [16]. For example, the visual system provides information on the position and motion of the body with respect to surrounding objects, and the somatosensory system provides position and motion information

* Corresponding author at: Department of Physical Medicine and Rehabilitation, Tohoku University Graduate School of Medicine, 2-1 Seiryo-machi, Aoba-ku, Sendai 980-8575, Japan. Tel.: +81 22 717 7338; fax: +81 22 717 7340.
E-mail address: izumis@bme.tohoku.ac.jp (S.-I. Izumi).

0966-6362/$ – see front matter © 2012 Elsevier B.V. All rights reserved.
doi:10.1016/j.gaitpost.2012.01.011

about the body with respect to the supporting surfaces [2,16]. For this reason, utilising this type of information is important for motor regulation. Among whole-body tasks, the sit-to-stand (STS) motion is one of the most mechanically demanding daily activities [7]. Centre of mass (COM) control is assumed to be a goal of postural responses [17]. Scholz et al. [18] suggested that the body COM is a control variable for the postural system quantitatively. COM control is important during STS, the period when the body mass is raised from relatively stable support to a position of lower mechanical stability [19].

This study aims to investigate the influence of visual and somatosensory constraints on COM control during STS. The concept of stability in the control-theoretical sense suggested by Scholz [20] was applied to evaluate COM control in this study. Using this concept, stability can be assessed experimentally by using the variability of the corresponding variable in time such as the fluctuation of a fixed point for postural states [21,22] or by using the reproducibility of that variable from trial to trial such as kinematics at matching points in time during movement [23]. Those are assumed to assess nervous system control. The lesser the value of the measured variable, the more the central nervous system controls that variable [20]. It was hypothesised that the variability in position and velocity of COM in the anterior–posterior and upward–downward directions, which are the major moving directions during STS, should be reduced when both visual and somatic senses are constrained during a critical controlling period.

2. Materials and methods

2.1. Participants

Twelve healthy adults aged 30.7 ± 6.4 years (six females and six males) participated in this study. Weight and height of the participants were 61.0 ± 11.4 kg and 167.7 ± 6.8 cm, respectively. None of the participants had a neurological disease or visual problems. All participants gave written consent, which was approved by the institutional ethics committee, before participating in the experiments.

2.2. Equipment and set-up

A MAC 3D System (Motion Analysis, Santa Rosa, CA, USA) motion measurement device and four force plates (ANIMA, Tokyo, Japan) were used to collect the experimental data. The system comprised eight infrared video cameras suspended from the ceiling. The error in the measurement volume was <2 mm for all cameras (length, 4 m; width, 4 m; height, 2 m). The *x*, *y*, and *z* axis represented the right–left, anterior–posterior, and upward–downward directions, respectively. The right, anterior, and upward directions were defined as positive directions.

Spherical markers with a diameter of 19 mm and covered with retro-reflective tape were attached to the following anatomical landmarks: (1) base of the fifth metatarsal in both feet, (2) both lateral malleoli, (3) both lateral femoral condyles, (4) both hip joints (1/3 distance from the greater trochanter to the anterior superior iliac spine), (5) anterior superior iliac supine, (6) posterior superior iliac supine, (7) both acromion processes, (8) right scapula (dummy was placed for distinguishing right from left), (9) spinous process of the second thoracic vertebra, (10) point anterior to the external auditory meatuses on both sides, and (11) glabbela.

A stool was placed on both the back plates so that the participant's feet could be placed separately on both the front plates. The force plate signals were sampled with an analogue–digital converter. Data from the video cameras and force plates were sampled at 120 Hz and were synchronised.

2.3. Experimental procedure

Participants performed STS 10 times under each of four different perceptual conditions; namely, normal (NO), vision restricted (VR), somatosensory restricted (SR) and vision and somatosensory restricted (VSR) conditions. The VR and SR conditions were set by instructing the participants to close their eyes and by placing an unstable wooden board on the participants' stool, respectively. The size of the unstable wooden board was 300 mm in length and 500 mm in width. A hemispherical rocker, 165 mm in diameter and 40 mm in height, was attached to the centre of the undersurface of the board. Although somatic sense was restricted only until the buttocks lifted off from the seating surface, this condition was assumed to affect the total movement according to the importance of the initial position in motor planning [24]. The measurement order of the four conditions was randomised among participants.

For all conditions, the height of the seating surface was matched to the fibular head. The distance maintained between the heels of the participants was equivalent to two-thirds the length of the participant's foot. Approximately half the thigh was in contact with the stool, and the knees were flexed at approximately 100°. The participants were instructed to loosely hang their arms at their sides without allowing them to contact the stool or their body throughout STS.

Before the measurement, the participants were instructed to move naturally from a sitting to a standing position at their preferred speed of movement. Immediately after the participants had assumed a seated posture in which they felt comfortable and steady, a buzzer was sounded and the measurements were initiated. After keeping the sitting position for 10 s to establish the perception of initial orientation [17], the second buzzer was sounded as a start sign of the movement. The participants were asked to maintain their posture after standing up until the third buzzer sounded, which was approximately 3 s later as a previous study [14]. After all the experimental trials, the participants were asked to describe differences in difficulties encountered or anxiety experienced during STS under the four conditions.

2.4. Data reduction and analysis

The coordinate of each reflective marker measured by the MAC 3D System was low-pass filtered using measurement software (EVaRT 5.0.4, Motion Analysis) with a 6 Hz cut-off frequency (bi-directional second-order, Butterworth digital filter). The location of the total COM was calculated based on body segment length [25] with adjustment for Japanese body proportion [26]. The position and velocity of COM and the force plate signals were low-pass filtered at 8 Hz using a finite impulse response filter. We used analysis software to reduce data (KineAnalyzer, KISSEI COMTEC, Nagano, Japan).

Onset of movement was defined as the first upward deviation from baseline in the COM acceleration traces in the *y* direction. This timing corresponded with the beginning of the centre of pressure (COP) retrogression. The end of the movement was defined as the first change from positive to negative in the differential value of the *z*-axis element in the ground reaction force (*Fz*) after reaching a plateau in the standing COM position. The time when the buttocks lifted off from the seat was defined as the time when the reaction force signal from the stool had expired. The time taken for the movement from onset to the end was normalised to one hundred percent (Fig. 1).

The standard deviation (SD) value of the COM position and velocity in the *x*, *y*, and *z* directions across 10 trials was obtained at each 1% of movement time. Then, the SD value of each kinematic parameter was integrated as a measure of variability with respect to COM control during the specific analysis period, which was the period from maximum COM velocity in the *y* direction (T1) to maximum COM velocity in the *z* direction (T2) (Fig. 1). During this period, COM simultaneously was applied a braking force in the *y* direction and a rising force in the *z* direction (Fig. 2). Fig. 3 demonstrates an example of SD integrals of the COM velocity in the *y* direction for two conditions (NO and VSR) in one participant. Each SD value was calculated from the results of 10 trials under the NO (Fig. 3a) and VSR conditions (Fig. 3b). Subsequently, the SD integral under the VSR condition, which was computed from

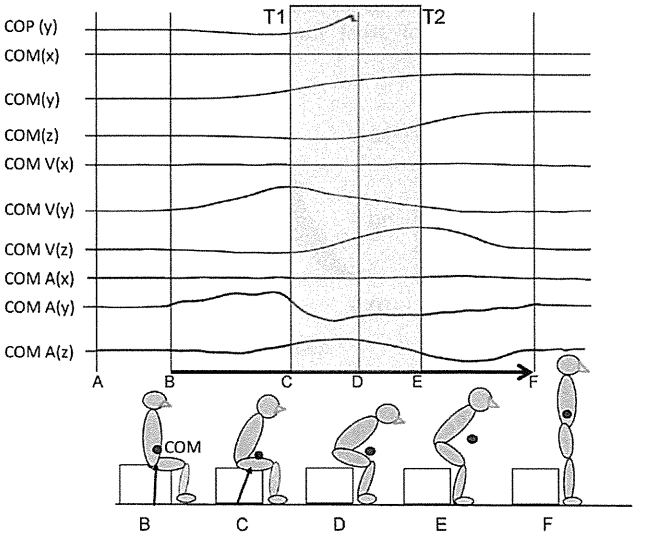

Fig. 1. Schematic time series of COP (*y* direction), which was measured by force plates under the chair, and centre of mass (COM) kinematics (position, velocity, and acceleration in the *x*, *y*, and *z* directions). The right, anterior, and upward directions were defined as positive directions. The period from B to F is defined as movement time for STS (A) start sign with sound, (B) STS initiated, (C) peak velocity in the *y* direction (D) thigh off, (E) peak velocity in the *z* direction, and (F) STS completed. The movement time is normalised to one hundred percent. The shaded area from C to D is defined as the analysis period. Arrows indicate ground reaction vectors of the force plates under the chair.

Please cite this article in press as: Kuramatsu Y, et al. Influence of constrained visual and somatic senses on controlling centre of mass during sit-to-stand. Gait Posture (2012), doi:10.1016/j.gaitpost.2012.01.011

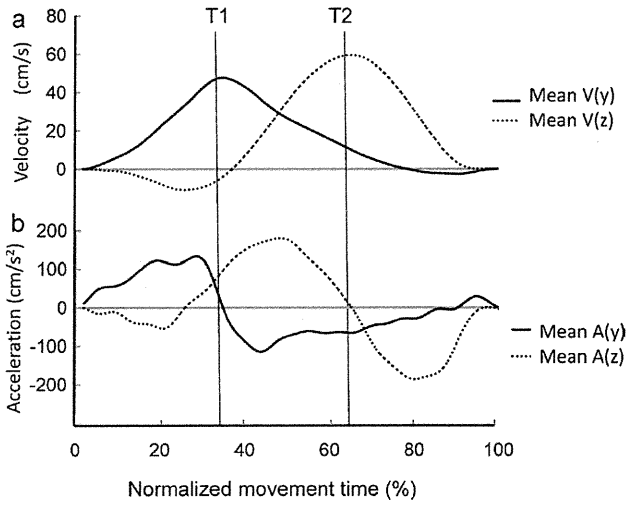

Fig. 2. Determining the period of comparing variability (example of one participant): (a) the time series of the centre of mass (COM) velocities (y and z directions) and (b) the time series of the COM accelerations (y and z directions). T1, the time point when COM velocity (y direction) was maximum; T2, the time point when COM velocity (z direction) was maximum.

T1 to T2, was smaller than that under the NO condition (Fig. 3c). In this manner, the SD integrals of the COM position and velocity in the three directions were calculated for all participants and subsequently compared among the four conditions.

The integrated SD data were statistically analysed with SPSS version 15 (SPSS Inc., Chicago, IL, USA). A one-way repeated-measures analysis of variance was performed to examine the difference in the integrated SD values of COM position and velocity for each direction among the four conditions. Post hoc multiple comparisons were performed using Bonferroni's adjustment. The significance level was set at 0.05.

3. Results

3.1. Experimental task achievement

There were no participants who felt anxiety, and all participants maintained their balance in all trials. Four trials were deemed unsuccessful because of stool movement, starting before the buzzer and unclear end of movement. Because those trials were eliminated, 476 of the 480 trials in12 participants were analysed.

The mean movement time was 1120–2440 ms, whereas the mean SD of the movement time was 90–190 ms. The variability within individual participants was much smaller than the variability among participants. No significant differences were observed in the time taken for STS movements under all four conditions ($p = 0.221$).

No significant differences were observed in the peak velocity in the z direction ($p = 0.316$), although significant differences were observed in the y direction between conditions of unrestricted and restricted somatic senses ($p < 0.05$). No bell-shaped velocity profile was observed in the x direction.

The average of the time points (across the trials and participants) ranged from 35% to 45% in T1 and from 58% to 71% in T2. SD of the T1 and T2 time points for the four conditions was about 1% (50 ms or shorter) of the movement time within a participant. The seat-off timing was 49.3% (SD 2.1) across all trials for all participants (Table 1).

3.2. Variability in the COM velocity and position

Significant differences were observed in the SD integral of the COM velocity in the y ($p < 0.05$) and z ($p < 0.05$) directions during the analysis period. The SD integral under the VSR condition was smaller than that under the NO condition (Fig. 4a and b). Significant differences were also observed in the SD integral of the COM position in the x direction ($p < 0.05$), where a significant difference was observed between the SD integral under the SR and NO conditions ($p < 0.05$). The SD integral increased for the COM position under the condition of perceptual constraint (Fig. 4c). No significant difference was observed in velocity in the x direction or in position in the y and z directions under all four conditions. No significant differences were observed in the COP position in the x and y directions.

4. Discussion

In this experiment, the length of the movement time and timing of T1 and T2 was almost the same within each participant for all

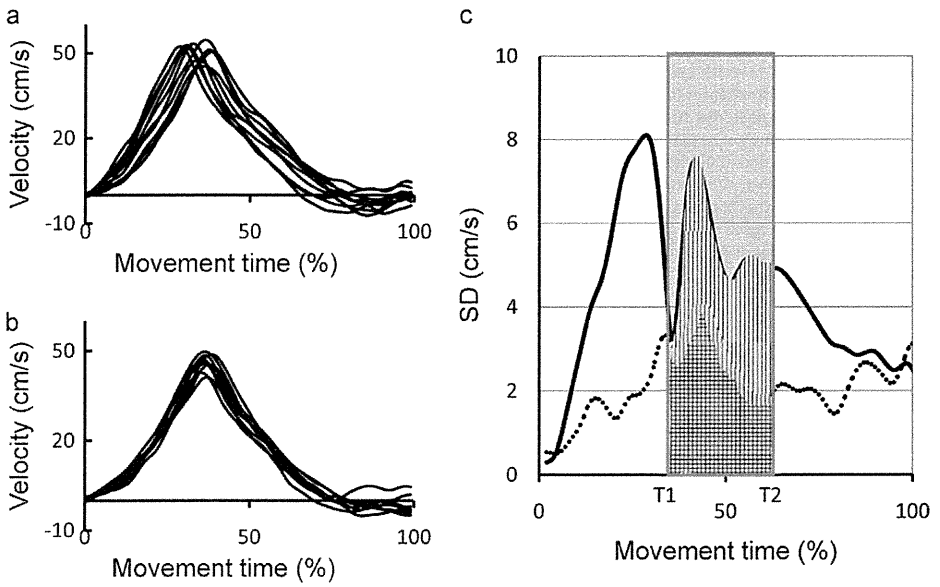

Fig. 3. Example of the variability in the y direction velocity: (a) velocity during the 10 trials under the normal (NO) condition, (b) velocity during the 10 trials in the vision- and somatosensory-restricted (VSR) condition, and (c) SD values of velocity for the two experimental conditions. Solid line indicates the NO condition. Dashed line indicates the VSR condition. They are calculated in the shaded area as the period from T1 to T2.

Please cite this article in press as: Kuramatsu Y, et al. Influence of constrained visual and somatic senses on controlling centre of mass during sit-to-stand. Gait Posture (2012), doi:10.1016/j.gaitpost.2012.01.011

Table 1
Mean values (standard deviation) of movement time, centre of mass (COM) velocity (*y* and *z* direction), and timing of events under each condition.

Condition	Movement time (s)	Peak *Vy* (cm/s)	Peak *Vz* (cm/s)	Timing of T1 (%)	Timing of T2 (%)	Timing of lift off (%)
NO	1.68 (0.33)	48.6 (5.6)	62.5 (13.2)	37.9 (3.6)	63.0 (3.8)	50.4 (3.5)
VR	1.74 (0.37)	47.8 (6.4)	60.8 (14.9)	38.0 (3.6)	63.6 (5.0)	50.7 (3.8)
SR	1.76 (0.34)	44.1 (7.1)	57.8 (12.7)	37.7 (2.7)	63.4 (4.0)	47.8 (3.1)
VSR	1.75 (0.36)	44.7 (7.4)	60.1 (14.3)	37.9 (2.9)	63.6 (4.1)	48.5 (3.5)
Total	1.73 (0.34)	46.3 (6.6)	60.3 (13.8)	37.9 (3.2)	63.4 (4.2)	49.3 (3.1)

NO, normal condition; VR, vision restricted condition; SR, somatosensory restricted condition; VSR, vision and somatosensory restricted condition; T1, time point when COM velocity (*y* direction) was maximum; T2, time point when COM velocity (*z* direction) was maximum.

four conditions. This finding suggests that the unstable wooden board did not affect performance despite various perceptual constraints. During STS, COM was accelerated forward in the sitting position before T1 and was decelerated upward within the base of support in the standing position after T2. Movements during both periods were relatively stable and simple. However, between the T1 and T2 periods, COM simultaneously decelerated forward and accelerated upward. Additionally, the support surface changed during the analysis period. These results demonstrate that variability in the COM velocity decreased more during this critical period when the two modalities (visual and somatic) were constrained. Kuniyoshi et al. [27] proposed that human body dynamics have both relatively stable regions (stable and simple movement periods) and relatively unstable regions (unstable and critical movement periods), and that human behaviour may realise motion by exploiting stable regions for reducing control signals and by applying intensive control only during the unstable regions. Our results corresponded to this proposition.

Constraining one modality did not significantly decrease the variability in COM kinematics, although the COM velocity was more controlled during the specific period (T1–T2) under the condition that constrained both modalities. A previous study demonstrated no significant differences in the variability in COM velocity and position by changing the support surface conditions, although a difference was demonstrated by only uncontrolled manifold analysis [14]. It may be difficult to detect the effect of perceptual constraints by intervening only one modality. This is because perceptual systems are redundant; in addition, there is a complementary relationship between the visual and somatosensory systems [2].

Our results demonstrated that variability in the COM velocity decreased significantly in the anterior–posterior and upward–downward directions under more severe perceptual constraints, whereas variability in the COM position in the right–left direction increased under similar conditions. Our findings correspond to the uncontrolled manifold hypothesis [28] and the optimal feedback control hypothesis [29]. These hypotheses concerning skilled performance postulate that variability is reduced in the direction where accuracy is most required and is allowed to increase in the other direction under a task-constrained situation. Our findings suggest that control of the COM velocity, which is more reliable information for postural control than position and acceleration [30], was enhanced in the major moving directions (anterior and upward directions) during the critical period when the two modalities of perception with respect to postural orientation (visual and somatic) were constrained.

One of the reasons why variability in the right–left direction was allowed to increase may be because healthy people use both legs as an actuator and a supporter. Therefore, participants could have executed STS movements with loading either on the left or right foot. Additionally the participants could move with similar timing and speed irrespective of changes in the loading side during trials, which may have resulted in a difference in COM position without a difference in COM velocity.

This study had a few limitations. First, only STS motion was investigated to understand the interaction between perception and whole-body movements. Thus, it will be necessary to research other movements to confirm further applications. Second, only variability in COM kinematics was analysed in this study. Further investigations regarding the initial posture, time series of joint angles or torques during movements and a quantification of the coordinative structure among joints should be considered for a more specific understanding of the perceptual effects on STS. Third, the degree of perceptual constraint was not the same between visual and somatic senses and did not exactly reflect the perceptual constraint in actual patients.

In conclusion, the nervous system sets priorities for COM control in the moving direction to accomplish STS motion under vision- and somatosensory-restricted conditions. These motor

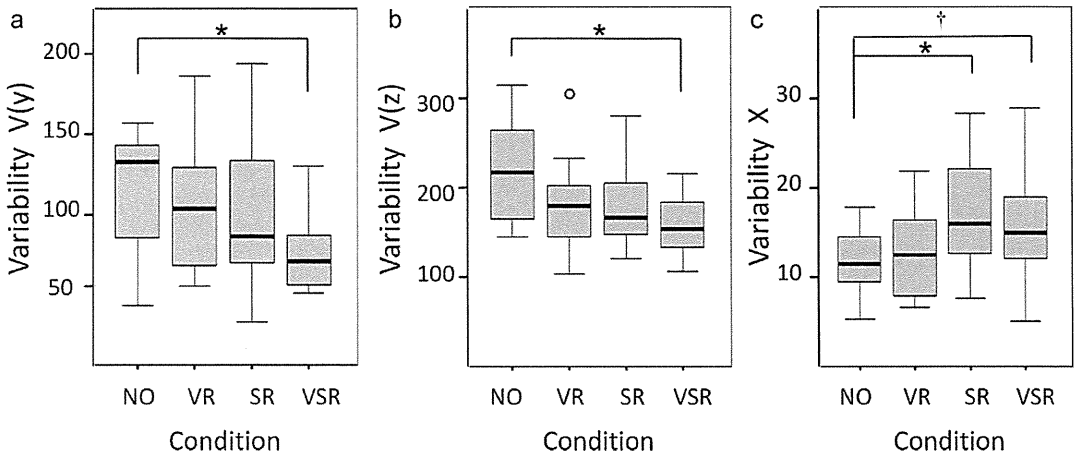

Fig. 4. Variability in centre of mass (COM) kinematics under the four experimental conditions that was calculated as an SD integral value during the T1–T2 period: (a) variability in velocity (*y* direction), (b) variability in velocity (*z* direction), and (c) variability in position (*x* direction). Boxes represent the interquartile range, cross bars in the boxes represent the median, the lengths of the whisker are within 1.5 times the box size, and the small circle represents an outlier. $^{*}p < 0.05$; $^{\dagger}p = 0.065$.

Please cite this article in press as: Kuramatsu Y, et al. Influence of constrained visual and somatic senses on controlling centre of mass during sit-to-stand. Gait Posture (2012), doi:10.1016/j.gaitpost.2012.01.011

regulations with perceptual constraints may facilitate better adaptation to changes in body and environmental conditions during daily life. An assessment of the relationship between perceptual constraints and motor regulation in patients with movement disorders may be needed because these disorders can lead to falls or cause difficulty in performing motor tasks.

Acknowledgements

We would like to thank Mr Akira Motokawa and Ms Rikako Isawa for their assistance with data collection, Dr Sumiko Yamamoto, Mr Takeshi Seki, Dr. Sanae Asahara, Mr Kazunori Sasaki and Dr Yoshinobu Ehara for their technical advice, and Dr Kazutoshi Kudo, Dr Haruhiko Sato, Dr Motoko Tanabe, Dr Yoshito Furusawa and Dr Yoshimi Suzukamo for their helpful comments.

Conflict of interest statement

None.

References

[1] Bernstein NA. On dexterity and its developments. In: Latash ML, Turvey MT, editors. Dexterity and its development. Mahwah, NJ: Lawrence Erlbaum Associates; 1996. p. 3–244.
[2] Shumway-Cook A, Woollacott. Motor Control: translating research into clinical practice, 3rd ed., Philadelphia: Lippincott Williams & Wilkins; 2007.
[3] de Rugy A, Montagne G, Buekers MJ, Laurent M. The control of human locomotor pointing under restricted informational conditions. Neurosci Lett 2000;281:87–90.
[4] Wolpert DM, Flanagan JR. Motor prediction. Curr Biol 2001;11:729–32.
[5] Vaugoyeau M, Hakam H, Azulay JP. Proprioceptive impairment and postural orientation control in Parkinson's disease. Hum Mov Sci 2011;30:405–14.
[6] Serino A, De Filippo L, Casavecchia C, Coccia M, Shiffrar M, Ladavas E. Lesion to the motor system affect action perception. J Cogn Neurosci 2010;22:413–26.
[7] Carr JH, Shephard RB. Stroke rehabilitation: guidelines for exercise and training to optimize motor skill. Edinburgh: Butterworth Heinemann; 2003.
[8] Kuo AD, Speers RA, Peterka RJ, Horak FB. Effect of altered sensory conditions on multivariate descriptors of human postural sway. Exp Brain Res 1998;122: 185–95.
[9] Gautier G, Thouvarecq R, Vuillerme N. Postural control and perceptive configuration: influence of expertise in gymnastics. Gait Posture 2008;28:46–51.
[10] Medina J, Jax SA, Brown MJ, Cslett HB. Contributions of efference copy to limb localization: evidence from deafferentation. Brain Res 2010;1355:104–11.
[11] Rossetti Y, Desmurget M, Prablanc C. Vectorial coding of movement: vision, proprioception, or both? J Neurophysiol 1995;74:457–63.
[12] Riley PO, Shenkman ML, Mann RW, Hodge WA. Mechanics of a constrained chair rise. J Biomech 1991;24:77–85.
[13] Kuo YL, Tully EA, Galea MP. Kinematics of sagittal spine and lower limb movement in healthy older adults during sit-to-stand from two seat heights. Spine 2010;35:E1–7.
[14] Reisman D, Scholz JP, Schoner G. Coordination underlying the control of whole body momentum during sit-to-stand. Gait Posture 2002;15:45–55.
[15] Bernstein NA. The coordination and regulation of movements. Oxford: Pergamon; 1967.
[16] Horak FB, Macpherson JM. Postural orientation and equilibrium. In: Shepherd J, Rowell L, editors. Handbook of physiology, section 12. Exercise: regulation and integration of multiple systems. New York: Oxford University; 1996. p. 255–92.
[17] Peterka RJ, Loughlin PJ. Dynamic regulation of sensorimotor integration in human posture control. J Neurophysiol 2004;91:410–23.
[18] Scholz JP, Schoner G, Hsu WL, Jeka JJ, Horak F, Martin V. Motor equivalent control of the centre of mass in response to support surface perturbations. Exp Brain Res 2007;180:163–79.
[19] Schenkman M, Berger RA, Riley PO, Mann RW, Hodge WA. Whole-body movements during rising to standing from sitting. Phys Ther 1990;10: 638–51.
[20] Schoner G. Recent development and problems in human movement science and their conceptual implications. Ecol Psychol 1995;8:291–314.
[21] Scholz JP, Kelso JAS. A quantitative approach to understanding the formation and change of coordinated movement patterns. J Mot Behav 1989;21: 122–44.
[22] Scholz JP, Kelso JAS, Schoner G. Nonequilibrium phase transition in coordinated biological motion: critical slowing down and switching time. Phys Lett A 1987;123:390–4.
[23] Schoner G. A dynamic theory of coordination of discrete movement. Biol Cybern 1990;63:257–70.
[24] Khoshnoodi MA, Motiei-langroudi R, Omrani M, Ghaderi-pakdell F, Abbassian AH. Kinesthetic memory in distance reproduction task: importance of initial hand position information. Exp Brain Res 2006;170:312–9.
[25] Winter DA. Biomechanics and motor control of human movement. New York: John Wiley & Sons; 1990.
[26] Suggested by Clinical Gait Analysis Forum of Japan. URL: http://wwwnejp/asahi/gait/analysis/comparison99/DIFF-SPEC-Jpdf.
[27] Kuniyoshi Y, Ohmura Y, Terada K, Nagakubo A, Eitoku S, Yamamoto T. Embodied basis of invariant features in execution and perception of whole body dynamics actions – knacks and focuses of roll-and-rise motion. Robot Auton Syst 2004;48:189–201.
[28] Scholz JP, Schoner G. The uncontrolled manifold concept. Identifying control variables for a functional task. Exp Brain Res 1999;126:289–306.
[29] Todorov E, Jordan MI. Optimal feedback control as a theory of motor coordination. Nat Neurosci 2002;5:1226–35.
[30] Jeka J, Kiemal T, Creath R, Horak F, Peterka R. Controlling human upright posture: velocity information is more accurate than position or acceleration. J Neurophysiol 2004;92:2368–79.

Please cite this article in press as: Kuramatsu Y, et al. Influence of constrained visual and somatic senses on controlling centre of mass during sit-to-stand. Gait Posture (2012), doi:10.1016/j.gaitpost.2012.01.011